WHAT VOLATILITY REVEALS: AGNOSTIC IDENTIFICATION OF EXCHANGE RATE AND TREASURY-MARKET DYNAMICS IN INCONVENIENT TIMES

2026

BANCO DE ESPAÑA
Eurosistema

Documentos de Trabajo
N.º 2629

Lucas ter Steege and Sofia Velasco

WHAT VOLATILITY REVEALS: AGNOSTIC IDENTIFICATION OF EXCHANGE RATE AND TREASURY-MARKET DYNAMICS IN INCONVENIENT TIMES

WHAT VOLATILITY REVEALS: AGNOSTIC IDENTIFICATION OF EXCHANGE RATE AND TREASURY-MARKET DYNAMICS IN INCONVENIENT TIMES (*)

Lucas ter Steege (**)

DEUTSCHE BUNDESBANK

Sofia Velasco (***)

BANCO DE ESPAÑA

(*) The views expressed in this paper are those of the authors and do not necessarily reflect the views of the Deutsche Bundesbank, the Banco de España or the Eurosystem. We would like to thank Benjamin Born, Marek Jarocinski, Maximilian Konradt, Elmar Mertens, seminar participants at the Banco de España, the Deutsche Bundesbank and the European Central Bank (IPA Economic Meeting) and conference participants at the Third International Conference on the Climate-Macro-Finance Interface (SAFE, RCEA) and at the 2026 Second WIRE Annual Workshop for their useful comments and suggestions.
(**) lucas.ter.steege@bundesbank.de
(***) sofia.velasco@bde.es

Documentos de Trabajo. N.º 2629

September 2026

https://doi.org/10.53479/44413

ISSN: 1579-8666 (online edition)

Abstract

This paper studies the financial-market transmission of the April 2025 U.S. tariff announcements, with a particular focus on the unusual combination of dollar depreciation and rising long-term U.S. Treasury yields. We ask whether the market reaction can be understood as the propagation of a single tariff-announcement shock or whether it instead reflects the interaction of distinct macro-financial disturbances. To address this question, we exploit time variation in the volatility and excess kurtosis of structural shocks to recover macro-financial forces without imposing event-based restrictions or exclusion assumptions. Our results show that the initial market reaction is consistent with a conventional safe-haven shock, but this mechanism cannot account for the subsequent joint behaviour of exchange rates and long-term U.S. Treasury yields. Instead, different segments of financial markets are dominated by distinct orthogonal shocks associated with safe-haven demand, confidence in U.S. institutions, Treasury-market intermediation and changes in the convenience value of dollar-denominated safe assets.

Keywords: exchange rates, Treasury yields, risk premia, trade policy shocks, safe-haven dynamics, heteroskedastic identification, financial spillovers.

JEL classification: F31, F41, G14, E44, C32.

Resumen

En este documento se estudia la transmisión de los anuncios arancelarios de Estados Unidos de abril de 2025 en los mercados financieros, con especial atención a la inusual combinación de depreciación del dólar y aumento de los rendimientos de la deuda pública estadounidense a largo plazo. Para ello, explota la variación temporal de la volatilidad y de la curtosis de los *shocks* estructurales con el fin de identificar las perturbaciones macrofinancieras sin imponer restricciones de signo, supuestos de exclusión ni estrategias de identificación basadas en ventanas de eventos. Los resultados muestran que la reacción inicial de los mercados es coherente con un episodio convencional de búsqueda de activos refugio, pero que este mecanismo no basta para explicar la evolución conjunta del tipo de cambio y de los rendimientos de la deuda pública estadounidense. En cambio, distintos segmentos de los mercados financieros estuvieron dominados por *shocks* ortogonales asociados a la demanda de activos refugio, la confianza en las instituciones estadounidenses, la intermediación en el mercado de los títulos de deuda pública emitidos por el Departamento del Tesoro de los Estados Unidos y los cambios en el valor de conveniencia de los activos seguros denominados en dólares. Estos resultados ponen de manifiesto que la respuesta de los mercados al episodio de abril de 2025 reflejó la interacción de varios mecanismos macrofinancieros, en lugar de la propagación de un único *shock* asociado al anuncio de los aranceles.

Palabras clave: tipos de cambio, rendimientos de la deuda pública, primas de riesgo, *shocks* de política comercial, activos refugio, identificación mediante heterocedasticidad, contagio financiero.

Códigos JEL: F31, F41, G14, E44, C32.

1 Introduction

On 2 April 2025, the U.S. administration announced a broad package of tariffs, proposing one of the largest increases in trade barriers in recent history.[1] The announcement triggered large movements across global financial markets. While some of these reactions were consistent with a rise in uncertainty—equity prices declined and volatility increased—others were more difficult to reconcile with conventional safe-haven dynamics. In the weeks that followed, the U.S. dollar depreciated against major currencies while long-term U.S. Treasury yields rose sharply. These unusual co-movements are particularly striking given the privileged role of the U.S. dollar and U.S. Treasuries in the international monetary system. Traditionally, episodes of heightened uncertainty have been associated with dollar appreciation and lower Treasury yields. The 2025 tariff episode therefore raises the possibility that exchange-rate and Treasury-market dynamics were driven by forces extending beyond a conventional tariff-announcement shock, potentially reflecting changes in the convenience value attached to dollar assets and U.S. Treasuries.

The privileged international role of the U.S. dollar is reflected in several interconnected features of the international monetary system. Dollar-denominated safe assets command unusually low expected returns because investors value their liquidity, safety, and collateral services (Du et al., 2018a; Krishnamurthy and Lustig, 2019). Dollar liabilities also occupy a dominant position in global funding markets and international balance sheets (Cetorelli and Goldberg, 2012; Shin, 2012; Ivashina et al., 2015; Bruno and Shin, 2017; Maggiori et al., 2020). Theoretical work further emphasizes that the dollar's role as a unit of account in trade invoicing is complementary to its role as a safe store of value, helping to sustain its dominance in both trade and global finance (Gopinath and Stein, 2021). During episodes of heightened global uncertainty, investors have historically sought both dollar liquidity and U.S. Treasuries, resulting in a joint appreciation of the dollar and a decline in Treasury yields (Jiang et al., 2018, 2021). Together, these features underpin the international role of the dollar and the notion of U.S. exorbitant privilege (Gourinchas and Rey, 2007, 2022; Jiang et al., 2024b). Recent work further argues that the dollar exchange rate itself reflects the convenience value attached to dollar-denominated safe assets, linking movements in exchange rates directly to changes in the scarcity of dollar safe assets and the Treasury basis (Jiang et al., 2021, 2024a; Gopinath and Stein, 2021). Against this backdrop, the market developments following the April 2025 tariff announcement raise

[1] The measures, widely referred to as "Liberation Day", were implemented through Executive Order No. 14257 and included a 10% baseline tariff on imports from more than 180 countries together with additional reciprocal tariffs linked to bilateral trade imbalances.

the possibility that these different dimensions of international privilege did not move in tandem.

Aware that this episode represents only a snapshot, we view it as a rare opportunity to study forces that are often difficult to observe directly. The tariff announcement provides a focal point, but the subsequent dollar depreciation and rise in long-term Treasury yields may reflect several overlapping disturbances rather than a tariff shock alone. We therefore exploit variation in volatility over nearly two decades to recover macro-financial shocks without imposing sign restrictions, event-specific assumptions, or exclusion restrictions. We subsequently assign an economic interpretation to the recovered shocks based on their empirical transmission patterns together with the mechanisms emphasized in the literature. Our agnostic statistical identification strategy is particularly valuable because several recent theories can account for similar reduced-form movements in exchange rates and Treasury yields, yet attribute them to distinct structural mechanisms, including shifts in safe-haven demand, confidence in U.S. institutions, Treasury-market intermediation, and changes in the convenience value attached to dollar-denominated safe assets. Distinguishing between these mechanisms is economically important because similar asset-price movements need not imply a common underlying shock. Whether the episode reflects a single disturbance or several distinct structural shocks has fundamentally different implications for how we interpret the role of the dollar, U.S. Treasuries, and the transmission of global financial stress. The resulting impulse responses allow us to assign an economic interpretation to the statistically identified shocks, while the historical decomposition shows that these mechanisms are jointly required to explain the 2025 episode. A conventional *Safe-Haven shock* captures the familiar flight-to-safety pattern of weaker equity prices, dollar appreciation, and lower Treasury yields, accounting for the broad risk-off component of the episode, particularly in equity markets. However, it cannot explain the joint dollar depreciation and rise in long-term Treasury yields observed after the tariff announcement. Instead, these movements require additional shocks associated with a deterioration in U.S. institutional credibility and disruptions to Treasury-market intermediation. Taken together, the evidence suggests that the April 2025 episode did not reflect the breakdown of a single safe-haven mechanism. Rather, it revealed distinct dimensions of U.S. international privilege that are ordinarily difficult to disentangle empirically.

Interpreting these developments poses a challenge for existing frameworks of exchange-rate and Treasury-market determination. The joint depreciation of the dollar and increase in long-term Treasury yields following the tariff announcement contrasts sharply with the behaviour typically observed during episodes of heightened uncertainty. This combination is difficult to reconcile with canonical safe-haven dynamics, under which adverse shocks such as a unilateral increase in trade barriers are generally associated with dollar appreciation and declining Treasury yields. This pattern is well documented in the literature on global risk shocks, safe-haven currencies, and the global financial cycle, where increases in global risk premia systematically trigger a flight into dollar-denominated safe assets and U.S. Treasuries (Hossfeld and MacDonald, 2015; Georgiadis and Mehl, 2015; Rey, 2015; Jiang et al., 2018, 2021; Georgiadis et al., 2024). Standard open-economy theory predicts that tariffs imposed by a dominant-currency country should appreciate the domestic currency through expenditure-switching effects, particularly under dominant-currency pricing (Gopinath et al., 2020). Consistent with these predictions, earlier U.S. tariff episodes, including those of 2018–2019, were associated with dollar appreciation (Furceri et al., 2018; Jeanne and Son, 2024).

Importantly, the market reaction observed in the days and weeks following the April 2025 tariff announcement need not have been generated by the announcement alone. The emerging literature offers several competing interpretations. Pinter et al. (2025) show that tariff-announcement shocks explain much of the initial reaction in equities, volatility, commodity prices and short-term inflation compensation, but account for little of the persistent dollar depreciation and movements in long-term government bond yields, which they attribute to orthogonal shocks associated with Treasury-market dysfunction. Frankovic and Karau (2026) find that shocks to “U.S. confidence” account for much of the gold and exchange rate movements around the April 2025 event, as well as some of the observed stock market movements. Ostry et al. (2025) argue that once expected foreign retaliation is taken into account, the exchange-rate response is considerably less puzzling than the behaviour of long-term Treasury yields. Other contributions instead emphasize portfolio rebalancing away from U.S. assets, changes in foreign-investor hedging demand, or a reassessment of the convenience value attached to dollar-denominated safe assets and Treasury markets (Hartley and Rebucci, 2025; Ignatenko et al., 2025; Du et al., 2026). These competing interpretations imply similar movements in observed asset prices while reflecting fundamentally different underlying structural disturbances. Rather than identifying a tariff-specific shock, we therefore recover a set of macro-financial disturbances over the full sample and examine their contribution to the dynamics observed during the 2025 episode.

Figure 1 compares financial-market developments following the 2025 tariff announcement with those observed during the August 2019 tariff escalation. The comparison is informative because both episodes were associated with a deterioration in investor sentiment, yet the subsequent behaviour of key financial variables differed markedly. In both cases, equity prices declined on impact. However, unlike in 2019, the 2025 episode was characterised by a persistent depreciation of the U.S. dollar against the euro despite weaker equity markets. At the same time, long-term U.S. Treasury yields increased after the initial impact and remained elevated, while inflation compensation, measured by the one-year inflation swap rate, rose substantially. Relative to the benchmarks discussed above, this combination suggests that the 2025 episode reflected additional forces beyond a conventional tariff or global-risk shock.

Figure 1: Financial Market Developments around Major U.S. Tariff Announcements

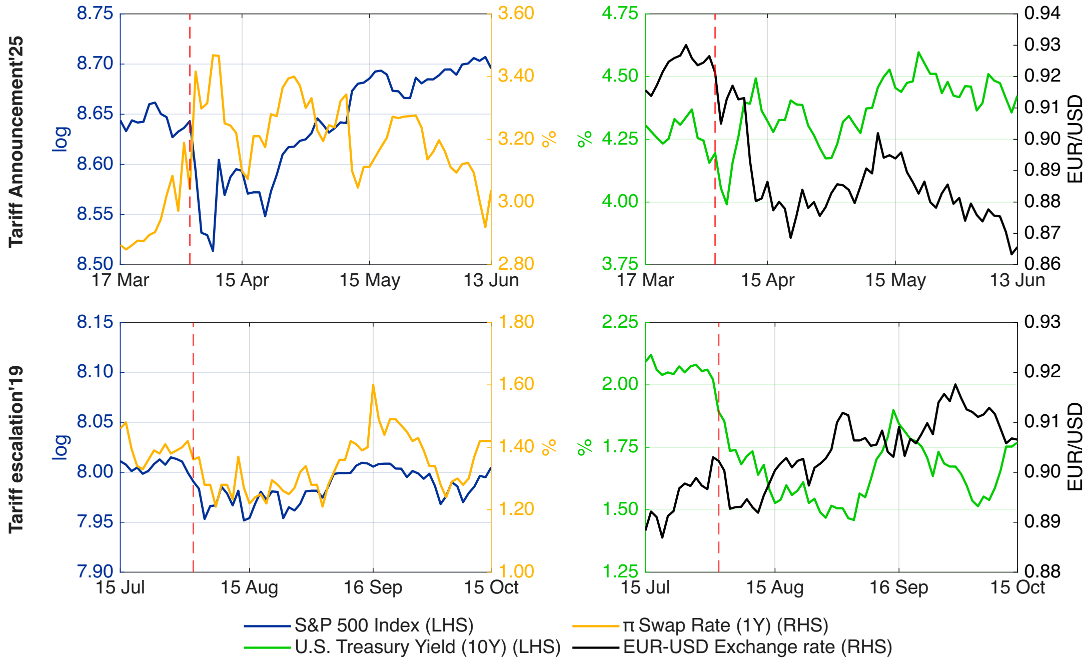

Notes: The figure compares four financial variables around the 2025 tariff announcements (15 March–13 June 2025) and the August 2019 tariff escalation (15 July–15 October 2019). The S&P 500 index and the EUR per USD exchange rate are reported in logs. The 1-year inflation swap rate and the 10-year U.S. Treasury yield are reported in percent. The 1-year inflation swap rate corresponds to the fixed rate exchanged against realized U.S. CPI inflation over a one-year horizon and serves as a market-based measure of short-term inflation compensation. The 10-year Treasury yield is the market yield on U.S. Treasury securities at constant 10-year maturity, quoted on an investment basis. The EUR per USD exchange rate is expressed as euros per U.S. dollar, so an increase denotes a dollar appreciation. Vertical dashed lines denote major tariff-announcement dates: 2 April 2025 (top row); 1 August 2019 (bottom row).

Recent work increasingly views U.S. international privilege as comprising several distinct but related dimensions. In particular, the literature distinguishes between global demand for dollar-denominated safe assets, Treasury-market functioning, and the convenience value attached specifically to U.S. Treasuries. Although these mechanisms can generate similar movements in exchange rates and bond yields, they reflect different underlying economic forces and have become central to interpreting recent episodes of market stress.

Figure 2: Dollar and Treasury Convenience around Major U.S. Tariff Announcements

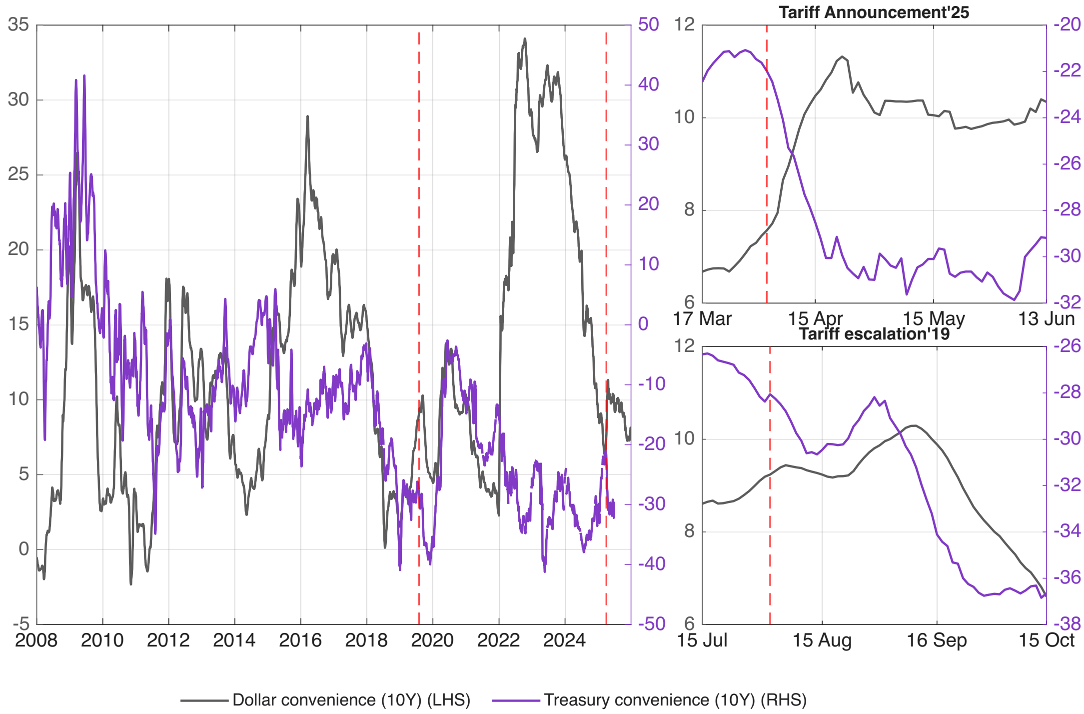

Notes: The figure compares two long-horizon convenience-yield measures over the estimation sample (2 July 2007–15 May 2025) and around two major tariff episodes. Dollar Convenience (10Y) measures the convenience value attached to holding long-term dollar-denominated safe assets after hedging exchange-rate risk (Du et al., 2026). Treasury Convenience (10Y) isolates the additional convenience value attached specifically to U.S. Treasury securities relative to other G10 government bonds (Du et al., 2018a, 2026). The left panel reports both series over the full estimation sample. The right panels compare their behaviour around the April 2025 tariff announcement (15 March–13 June 2025) and the August 2019 tariff escalation (15 July–15 October 2019). Both series are expressed in basis points. Vertical dashed lines denote the major tariff-announcement dates: 2 April 2025 and 1 August 2019.

Following the Global Financial Crisis, Treasury-market structure changed substantially. Regulatory reforms constrained dealer balance sheets while non-bank intermediaries assumed an increasingly important role in Treasury intermediation. The March 2020 Treasury-market turmoil exposed these structural vulnerabilities, demonstrating that Treasury-market functioning could deteriorate despite exceptionally strong global demand for dollar liquidity (Kashyap et al., 2025). Building on this evidence, Du et al. (2026) show that dollar convenience and Treasury convenience have become increasingly distinct dimensions of U.S. international privilege.

Figure 2 summarizes this evolution. The left panel shows that Dollar Convenience and Treasury Convenience broadly co-moved during the Global Financial Crisis and the European sovereign debt crisis but gradually diverged following the post-crisis restructuring of Treasury markets. The right panels compare the 2025 tariff episode with the 2019 tariff escalation. Unlike in 2019, the two measures moved in opposite directions during the 2025 episode, suggesting that investors reassessed different dimensions of U.S.

international privilege rather than uniformly reducing demand for U.S. safe assets.

This distinction motivates our empirical analysis. Rather than interpreting the 2025 episode as the realization of a single tariff or safe-haven shock, we allow separate structural disturbances to affect global safe-haven demand, confidence in U.S. institutions, and Treasury-market functioning. The historical decomposition subsequently shows that these mechanisms dominate different segments of financial markets, implying that the episode reflects the interaction of several orthogonal macro-financial shocks rather than the propagation of a single disturbance.

Our contribution relates to several strands of the literature. Structural models of tariff shocks impose economic mechanisms to discipline counterfactual outcomes (Kalemli-Özcan et al., 2025; Alessandria et al., 2025; Auclert et al., 2025; Rodríguez-Clare et al., 2025), but their implications for asset prices depend on assumptions about monetary policy, expectations, risk sharing, and the currency in which trade is invoiced. High-frequency event studies instead focus on narrow windows around announcements (Hartley and Rebucci, 2025; Ignatenko et al., 2025), isolating immediate valuation effects but typically abstracting from multi-shock dynamics. A close empirical benchmark is Pinter et al. (2025), who show that tariff-announcement shocks account for much of the initial market reaction, while the subsequent joint dynamics of the dollar and government bond yields are less tightly linked to the announcement itself. We build on this setting but depart from event-based identification by exploiting time variation in second moments over the full sample. This allows for a multi-shock environment in which safe-haven demand, dollar-asset pricing, and Treasury-market intermediation can be separated empirically rather than attributed ex ante to a single announcement shock. Methodologically, our framework builds on the heteroskedasticity-based identification approach of Rigobon (2003) and subsequent contributions. Identification arises from time variation in second moments: changes in the relative volatility of structural shocks allow the structural impact matrix to be recovered without exclusion restrictions. While non-Gaussianity can provide an additional source of identification through higher-order moments (Lanne et al., 2017; Jarocinski, 2024), in our setting it plays a complementary role by improving empirical fit and capturing the excess kurtosis present in financial data. This paper makes three contributions. First, we provide evidence that the financial-market dynamics following the April 2025 tariff announcement cannot be understood as the propagation of a single tariff or safe-haven shock. Instead, our historical decomposition shows that different components of the financial-market response were driven by distinct macro-financial shocks, including conventional safe-haven demand, changes in confidence in U.S. institutions, and

Treasury-market intermediation. Second, we demonstrate how heteroskedasticity-based identification can be used to recover these overlapping structural shocks without relying on sign restrictions, event windows, or exclusion restrictions. The empirical application illustrates how statistically identified shocks can subsequently be given an economic interpretation through their transmission patterns and historical contributions. Third, we show through a Monte Carlo simulation that the proposed identification strategy remains reliable across alternative variance specifications, provided that the data contain sufficiently informative variation in second moments, excess kurtosis, or both.

The remainder of the paper is organised as follows. Section 2 presents the empirical framework and identification strategy. Section 3 analyses the financial-market dynamics surrounding the 2025 tariff episode. Section 4 concludes.

2 Model

We consider a VAR model for N endogenous variables of order p:

$$y_t = b_0 + B_1 y_{t-1} + \ldots + B_p y_{t-p} + A^{-1}\epsilon_t \tag{1}$$

$$\epsilon_t|\omega_t \sim \mathcal{N}(0, \Omega_t), \quad \Omega_t = diag(\omega_{1,t}e^{h_{1,t}}, \ldots, \omega_{N,t}e^{h_{N,t}}) \tag{2}$$

$$\omega_{i,t} \sim \mathcal{IG}\left(\frac{\nu_i}{2}, \frac{\nu_i}{2}\right), \quad \nu_i > 0 \tag{3}$$

$$h_{i,t} = \rho_i h_{i,t-1} + v_{i,t}, \quad |\rho_i| < 1, \quad v_{i,t} \sim \mathcal{N}(0, \sigma_i^2) \tag{4}$$

$$h_{i,1} \sim \mathcal{N}\left(0, \frac{\sigma_i^2}{1-\rho_i^2}\right) \tag{5}$$

The model specifies each structural error $\epsilon_{i,t}$ as featuring both heavy tails as in Lanne et al. (2017), Brunnermeier et al. (2021), or Kociecki et al. (2025), and a stationary stochastic volatility component as in Chan et al. (2024). Without the stochastic volatility component the structural errors would follow a Student-t distribution, where the assumption $\nu_i > 0$ is enforced via the prior. The impact matrix containing the contemporaneous effects of the structural shocks, A^{-1}, is assumed to be invertible but otherwise unrestricted. As in Chan et al. (2024) our model is order-invariant, meaning that our estimates of individual volatilities and/or heavy tailedness do not depend on the specific ordering of the endogenous variables.

2.1 Estimation

We use Markov chain Monte Carlo (MCMC) methods to estimate the model because its posterior distribution is analytically intractable. Here we briefly outline the prior distributions and sampling steps; full details on the prior hyperparameters and Gibbs sampler are provided in Appendix A.3. Let $\Theta = (\alpha, \beta, \omega, \nu, \rho, \sigma^2, h)$ be the collection of parameters in the model. $\alpha = \text{vec}(A)$ contains the coefficients of the inverse impact matrix, β denotes the VAR slope coefficients and constants. The $NT \times 1$ vector ω contains the variance parameters related to the Student-t distribution, the $N \times 1$ vector ν collects the respective degrees of freedom. Lastly, ρ, σ^2, and h collect the parameters related to the N stochastic volatility processes. Our prior assumes independence between the parameter blocks.

The Gibbs sampler cycles through the following steps, where θ denotes the set of parameters other than the ones being sampled in the respective steps:

1. $p(\alpha|y, \theta) = p(\alpha|y, \beta, \omega, h)$
2. $p(\beta|y, \theta) = p(\beta|y, \alpha, \omega, h)$
3. $p(\omega|y, \theta) = \prod_{i=1}^{N} \prod_{t=1}^{T} p(\omega_{i,t}|y, \alpha, \beta, \nu_i, h_{i,t})$
4. $p(\nu|y, \theta) = \prod_{i=1}^{N} p(\nu_i|\omega_i)$
5. $p(\sigma^2|y, \theta) = \prod_{i=1}^{N} p(\sigma_i^2|\rho_i, h_i)$
6. $p(\rho|y, \theta) = \prod_{i=1}^{N} p(\rho_i|\sigma_i^2, h_i)$
7. $p(h|y, \theta) = \prod_{i=1}^{N} p(h_i|y, \alpha, \beta, \omega_i, \rho_i, \sigma_i^2)$

To sample α we use the algorithm in Chan et al. (2024) who build on earlier work by Waggoner and Zha (1999) and Villani (2009). For the last step we use the auxiliary mixture sampler from Kim et al. (1998). As noted in Del Negro and Primiceri (2015), it is important to sample the auxiliary mixture indicators before the log-volatilities are sampled to draw from the correct conditional posterior (see also Chan (2024)). In the spirit of Bertsche and Braun (2022) we remove the empirical mean from each draw for h_i during the posterior sampler which implicitly fixes the scale of the structural A matrix. We do so to avoid potential scaling issues in the posterior if no prior information on the scale of the structural shocks is supplied to the model. Most other steps of the sampler are standard, except for those related to ν_i and ρ_i. As these densities are univariate we use a Griddy-Gibbs step as in Ritter and Tanner (1992).

As is well known in this type of model, the order of the structural shocks and the columns of the impact matrix A^{-1} is arbitrary. Furthermore, it is always possible to flip the sign of a given column and the corresponding shock without changing the likelihood function of the model. Hence, a procedure is necessary to normalise the posterior draws to yield reliable inference. We combine the approaches by Kociecki et al. (2025) and Poworoznek et al. (2021) to do so. Having obtained the desired number of draws from the posterior, we use the efficient approach by Kociecki et al. (2025) to choose the sign-permutation of a given draw that minimizes the Frobenius norm between the permutation and a reference matrix. Instead of using the maximum likelihood estimator as the reference matrix we determine the reference point from the posterior sample itself based on the impact matrix with median condition number, in line with Poworoznek et al. (2021). They suggest to use the condition number as it proxies unique information contained in the columns of the impact matrix draws, based on which we wish to normalise the draws. Choosing the median then ensures that one uses a representative draw from the posterior. This is similar in spirit to choosing the maximum likelihood estimator as the reference point, provided that it is close to the posterior mode, which may not be the case in practice. Furthermore, the approach we use is much simpler to implement. We provide a detailed description in Appendix A.4.

2.2 Identification

In addition to being well suited to modelling financial time series, the model can be statistically identified when the structural shocks exhibit sufficient heteroskedasticity, excess kurtosis, or both. Specifically, Bertsche and Braun (2022) show that the model is fully identified if the shocks are mutually uncorrelated and $|\rho_i| \neq 0$ for $i = 1, \ldots, N-1$. A similar result obtains even if no heteroskedasticity is present but the shocks are independent and at most one has a Gaussian distribution. Below we investigate both features and indeed find that these identification results apply in our case. The intuition behind the identification result in the case of independent Student-t structural shocks is nicely illustrated in Jarocinski (2024), which applies to our model as well. When the shocks are Gaussian, the model can make use only of the first and second moments of the residual distribution. The classic identification problem then results from the fact that there are infinitely many ways to factor a given residual covariance matrix to produce an estimate for A^{-1} that the model cannot distinguish between, as all such factorizations are observationally equivalent. When the structural shocks have non-Gaussian distributions, however, excess kurtosis breaks this invariance. With a heavy-tailed shock distribution it sometimes happens that one shock obtains a large, outlying value while all other shocks obtain only small values. In this case the observed data are driven predominantly by one shock only, revealing its effects. This is similar in spirit to an event-study approach in which particular observations are known to be driven by specific forces only, which are thus identifiable from the observable data. The same intuition applies when identification arises from heteroskedasticity. Assume for simplicity the case of two structural shocks only, of which only one is heteroskedastic. The reason we can identify the shocks in this case is also the fact that the heteroskedastic shock will occasionally realize with a large value due to its inflated variance, thus being responsible for the bulk of the observed variation in this instance. A potential problem with this approach, however, is that identification is only statistical in nature, and the identified shocks may not carry economic meaning. To resolve this issue we inspect the impulse response functions of the model to attach economic meaning to the identified shocks.

2.3 Simulation evidence on statistical identification

In this section we complement the previous discussion with a Monte Carlo simulation of how identification through higher moments works in practice. The Monte Carlo analysis serves two complementary purposes. First, it evaluates how three estimated variance specifications—SV, t-Distribution, and SV-t—fit data generated under four specific data-generating processes in a fixed three-variable VAR design, using mean predictive log likelihoods and predictive log Bayes factors computed from sums of one-step-ahead predictive likelihoods, following Geweke and Amisano (2010). Second, it assesses whether the implied statistical identification delivers accurate structural inference by examining the recovery of impulse responses across those designs.

The simulation design keeps the reduced-form VAR dynamics and the impact matrix fixed across all simulation designs and varies only the distribution and variance dynamics of the structural shocks. We consider four data-generating processes: (i) independent stochastic volatility processes as in (A.4), (ii) Student-t shocks as in (A.3), (iii) a combination of stochastic volatility and Student-t shocks, and (iv) a Gaussian homoskedastic benchmark. The simulation is therefore informative about robustness across these specific environments rather than across every possible specification of the shock distribution.

The Monte Carlo simulation delivers two main findings. First, in terms of density evaluation, Bayesian model comparison favours specifications that capture the dominant source of heterogeneity in the structural shocks. The SV-t specification receives the strongest overall support, including under the SV-t data-generating process, and only slightly outperforms the simpler correctly specified models under the SV and t-Distribution designs. This likely reflects the greater flexibility of the SV-t model, which can accommodate both time variation in second moments and fat-tailed realisations. More generally, the results suggest that predictive likelihoods reward specifications that capture the main features of the shock distribution even when the exact data-generating process is unknown. This provides a rationale for adopting the SV-t specification in the empirical application, where the true shock process is likewise unobserved. Because the reported results are based on a finite number of Monte Carlo replications, small quantitative differences across specifications may vary somewhat with a larger simulation sample. The broad pattern of results, however, is stable across the replications considered.

Second, in terms of structural inference, we find that impulse responses are recovered accurately across the alternative estimated specifications whenever the data-generating process exhibits either non-Gaussianity or sufficiently rich variation in second moments. Importantly, the structural impact matrix can be recovered even when the estimated specification does not coincide with the true data-generating process. For example, when the true shocks are homoskedastic but exhibit excess kurtosis, the SV-only model still recovers the impulse responses accurately; conversely, the t-Distribution model performs well when identification is generated by stochastic volatility. By contrast, in the Gaussian homoskedastic benchmark, neither time variation in second moments nor excess kurtosis provides identifying information. The structural impact matrix is therefore not uniquely identified, and the recovery of impulse responses becomes substantially less reliable.

These findings are consistent with the argument in Sims (2021) that sufficiently rich second-moment heterogeneity renders the likelihood informative for both model comparison and identification. Overall, the Monte Carlo results show that identification is not tied to a particular volatility specification, but instead requires sufficiently informative variation in second moments, excess kurtosis, or both. This conclusion is corroborated by the empirical application to oil markets in Appendix C, where we replicate the benchmark results of Bertsche and Braun (2022) in a Bayesian framework under three alternative specifications of the variance dynamics: a t-Distribution model, an SV model, and an SV-t specification. Across all three variants, the estimated impulse responses closely match the frequentist benchmark, with only minor quantitative differences across specifications. Together, the Monte Carlo evidence and the empirical replication indicate that heteroskedastic identification remains robust across alternative variance specifications in applied settings.

3 Financial Market Dynamics Around the 2025 Tariff Announcement

We analyse financial-market dynamics around the April 2025 tariff announcement using a VAR with stochastic volatility and Student-t innovations. Consistent with the identification strategy introduced above, structural shocks are identified via higher moments induced by stochastic volatility and excess kurtosis, without imposing sign restrictions, exclusion restrictions, or event-specific assumptions (Rigobon, 2003; Bertsche and Braun, 2022). Our empirical design does not isolate a tariff-specific structural shock. Instead, we estimate a set of macro-financial shocks over the full sample and use them to decompose asset-price movements during the April 2025 tariff episode. This approach allows us to assess whether the observed dynamics can be attributed to a single dominant disturbance or instead reflect the interaction of multiple underlying shocks, including those unrelated to the initial tariff announcement.

The analysis uses daily data spanning 2 July 2007 to 15 May 2025. The complete set of series is reported in Appendix Table D.2. The baseline information set captures broad macro-financial conditions. The S&P 500 and the VIX measure global risk sentiment, the EUR per USD exchange rate captures the external value of the dollar, and the one-year inflation swap rate summarizes market-based inflation expectations. We further add the three-month Treasury term premium from the Adrian–Crump–Moench (ACM) model (Adrian et al., 2013), allowing us to distinguish changes in long-term Treasury yields arising from compensation for duration risk from those associated with changes in expected short rates. Together, these variables characterise the benchmark transmission of global risk, monetary-policy expectations, and exchange-rate dynamics emphasized in the literature on international macro-financial spillovers and recent tariff announcements (Habib and Stracca, 2012; Georgiadis et al., 2024; Pinter et al., 2025).

The second group of variables is designed to distinguish among competing explanations centered on the functioning of Treasury markets and the international role of dollar-denominated safe assets. The 10-year U.S. Treasury yield and the 10-year euro-area government bond yield capture the relative behaviour of long-term sovereign yields across the two currency areas. To measure Treasury-market intermediation more directly, we include the 10-year U.S. swap spread, which is closely linked to dealer balance-sheet capacity and limits to arbitrage (Boyarchenko et al., 2018; Kashyap et al., 2025). We further include two long-horizon covered interest parity (CIP) measures developed by Du et al. (2018a, 2026). Dollar Convenience (10Y) measures the convenience value attached to holding long-term dollar-denominated safe assets after hedging exchange-rate risk, reflecting the non-pecuniary services that investors derive from their liquidity, collateral value, and reserve-currency status. Treasury Convenience (10Y) instead isolates the additional convenience value attached specifically to U.S. Treasuries relative to other G10 government bonds. Recent work emphasizes that these two dimensions of U.S. international privilege need not move together, implying that broader demand for dollar assets and Treasury-specific demand may evolve independently during periods of market stress (Jiang et al., 2021, 2024a; Du et al., 2026).

Taken together, these variables allow us to distinguish between conventional risk-off dynamics, Treasury-market intermediation shocks, and changes in the convenience value attached to dollar-denominated reserve assets. This distinction is particularly valuable because these mechanisms often imply similar movements in exchange rates and long-term yields while generating markedly different predictions for swap spreads, Treasury term premia, and long-horizon CIP deviations.

Before turning to the effects of the identified shocks, we verify that the data display sufficient higher-moment variation to support identification. The estimated volatility processes are precisely measured, highly persistent, and display pronounced comovement during periods of market stress, most notably in early 2020 and again in March–April 2025. Appendix Figure D.5 reports the estimated stochastic volatility processes and the posterior distributions of the Student-t degrees-of-freedom parameters, while Appendix Figure D.6 reports trace plots for the normalised impact matrix.

3.1 Impulse responses

We now turn to the economic interpretation of the statistically identified shocks, characterising each shock through its combined effects on risk sentiment, exchange rates, Treasury yields, Treasury-market functioning, and the two dimensions of U.S. international privilege captured by Dollar Convenience and Treasury Convenience. This joint perspective is particularly informative because several competing explanations for the 2025 episode imply similar movements in exchange rates and long-term Treasury yields while differing markedly in their implications for Treasury-market intermediation and the convenience value attached to dollar-denominated safe assets. Figure 3 reports the impulse responses of the four statistically identified shocks that are most informative for understanding the dynamics surrounding the April 2025 tariff announcement. Their contributions to the episode are examined through the historical decomposition below. Following Jarocinski (2024), the effects are normalised using the empirical standard deviations of the structural shock series by multiplying the columns of the estimated impact matrices for each posterior draw by the estimated implied shock standard deviations. Appendix Figure D.7 reports the complete set of impulse responses.

The shock in the first row generates a decline in equity prices, a sharp increase in the VIX, an appreciation of the dollar, and lower U.S. Treasury yields. Short-term inflation compensation falls on impact, while euro-area long-term yields also decline, consistent with a broad-based flight into safe assets. Moreover, U.S. Treasury yields decline more strongly than euro-area yields, indicating a larger relative increase in demand for U.S. Treasuries than for euro-area government bonds. The resulting transmission closely matches the conventional risk-off pattern documented in the literature and captures the familiar safe-haven role of both the U.S. dollar and Treasuries. For these reasons we label this shock as a *Safe-Haven shock*. Treasury Convenience also declines modestly on impact. Although economically small, this response is consistent with recent evidence that the convenience value attached specifically to U.S. Treasuries has weakened relative to other dimensions of dollar safe-asset demand (Du et al., 2026).

To construct these impulse responses, we combine the first two structural shocks reported in Figure D.7 by summing the corresponding columns of the impact matrix. The two shocks have very similar effects across variables, with the main differences arising in the exchange rate and euro-area bond yields. The first shock leads to an appreciation of the U.S. dollar, whereas the second generates an economically small depreciation and has little impact on euro-area bond yields. We consider this aggregation justified because, taken together, the two shocks account for virtually all of the movements in stock prices and volatility around the tariff announcements we study and, as we show below, their combined contribution to the exchange rate remains limited relative to the other shocks.

Besides its impact on the variables in the system, we can also gain further insights into this shock by inspecting the corresponding volatility processes in Appendix Figure D.5, namely the first two shown there. The first volatility process features notable spikes between October and December 2008 during the Great Financial Crisis, between March and April 2020 at the onset of the global pandemic, and again in early April 2025. In all three episodes, stock prices plummeted, growth prospects deteriorated, and U.S. Treasury yields generally declined persistently. The second volatility process captures the same episodes but is more erratic in nature. This suggests that it is primarily associated with the VIX, reflecting a form of "volatility-in-volatility." It therefore seems likely that the estimated effects of this shock are largely informed by episodes typically associated with safe-haven dynamics, lending further support to our economic interpretation.

The shock in the second row of Figure 3 is characterised by an immediate depreciation of the U.S. dollar together with higher long-term U.S. Treasury yields and a pronounced deterioration in Dollar Convenience. At the same time, Treasury Convenience and swap spreads respond little, suggesting that the shock does not primarily reflect disruptions to Treasury-market functioning. Instead, the combination of a weaker dollar, higher compensation for holding long-term U.S. assets, and a decline in Dollar Convenience is consistent with a broad repricing of U.S. dollar assets. Following the discussion in the introduction, we interpret this pattern as reflecting a deterioration in confidence in the institutional and policy environment underpinning the international role of the United States. We therefore label this shock the *U.S. Institutional Credibility shock*.

The defining feature of the third shock is a pronounced deterioration in Treasury-market functioning. The shock generates a substantial widening of the negative swap spread together with a marked decline in Treasury Convenience, while leaving Dollar Convenience largely unaffected. The resulting transmission is consistent with disruptions in Treasury-market intermediation arising from constraints on dealer balance sheets and reduced arbitrage capacity, as emphasized in the recent literature on Treasury-market fragility (Boyarchenko et al., 2018; Kashyap et al., 2025; Du et al., 2026). At the same time, the shock appears largely unrelated to broader macroeconomic conditions or changes in the economic outlook, as neither equity prices, volatility, nor inflation expectations respond significantly. We therefore interpret this disturbance as a *Treasury Market Intermediation shock*.

Finally, the fourth row depicts a *Safe-Asset Convenience shock*. Unlike the previous shocks, it is characterised primarily by a sizable increase in both Dollar Convenience and Treasury Convenience, while the remaining macro-financial variables respond only modestly, if at all. The shock therefore captures changes in the non-pecuniary value that global investors attach to dollar-denominated safe assets, including their liquidity, collateral services, and reserve-currency role, rather than disruptions to Treasury-market functioning. This interpretation is consistent with recent work arguing that fluctuations in the convenience value of dollar-denominated safe assets constitute a distinct dimension of U.S. international privilege (Jiang et al., 2021; Du et al., 2026).

Figure 3: Impulse response functions

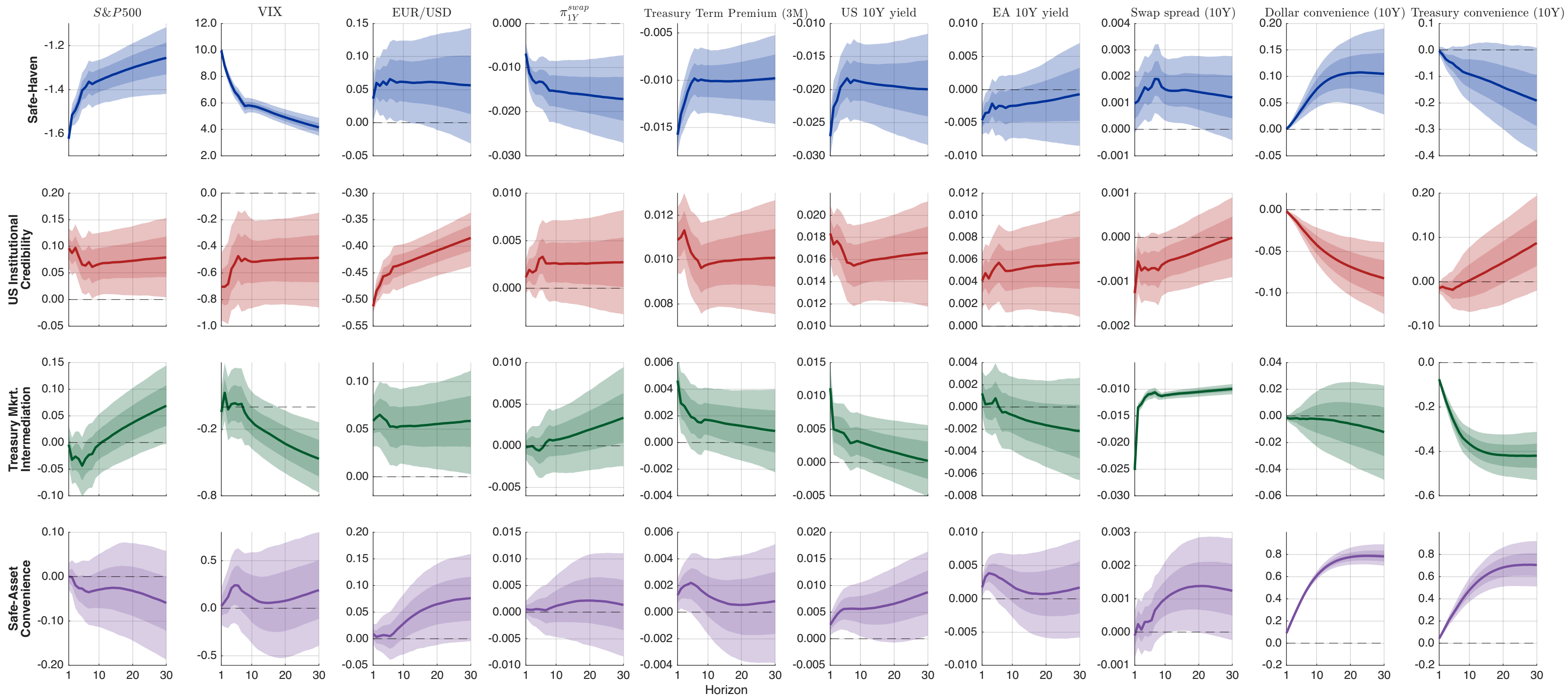

Notes: The figure reports impulse response functions over a 30-day horizon. Shaded areas denote 68% and 95% pointwise posterior credible intervals; the solid line is the posterior median. Rows show the *Safe-Haven shock* (shocks 1–2 combined), the *U.S. Institutional Credibility shock* (shock 3), the *Treasury Market Intermediation shock* (shock 8), and the *Safe-Asset Convenience shock* (shock 9).

3.2 Historical decompositions

The impulse responses characterise how each statistically identified shock propagates through financial markets. An equally important question, however, is whether these shocks actually explain the behaviour of asset prices during the April 2025 tariff episode that motivates the analysis. Figure 4 therefore reports the historical decomposition, which quantifies the contribution of each structural shock to the observed evolution of financial markets. The historical decomposition provides the central empirical test of our interpretation. If the economic labels assigned to the statistically identified shocks are meaningful, each shock should account primarily for the financial variables whose impulse responses motivated its interpretation. Conversely, if the episode reflected a single dominant tariff disturbance, the same shock would explain most variables simultaneously. The evidence strongly supports the former interpretation. Different components of the financial-market response are dominated by different structural shocks, implying that the 2025 episode reflects the interaction of several orthogonal macro-financial forces rather than the propagation of a single disturbance.

The first result concerns the broad risk-off component of the episode. The decline in equity prices and the increase in implied volatility are explained predominantly by the *Safe-Haven shock*, consistent with the response identified in recent event-study evidence (Pinter et al., 2025). Thus, the decomposition confirms that conventional flight-to-safety forces account for the behaviour of equity markets. Furthermore, as noted in the introduction, the initial days of the April 2025 episode saw falling U.S. Treasury yields, as expected during a traditional safe-haven episode, and our first shock accounts for this pattern. The main empirical puzzle therefore does not lie in the equity-market response, but in the joint behaviour of exchange rates and fixed-income markets. The second result concerns the central empirical puzzle motivating the paper. Unlike equity markets, neither the depreciation of the dollar nor the increase in long-term Treasury yields following the initial impact is explained by the *Safe-Haven shock*. Instead, both movements are primarily associated with the *U.S. Institutional Credibility shock*, which accounts for the bulk of the rise in the term premium and long-term Treasury yields and, strikingly, for nearly all of the observed exchange-rate depreciation. In this respect, our identified shock bears some resemblance to the “U.S. confidence” shock identified by Frankovic and Karau (2026). At the same time, our decomposition separates the response of equity markets from that of exchange rates and fixed-income markets, rather than attributing all of these movements to a single disturbance. The evidence therefore indicates that the unusual combination

Figure 4: Historical decomposition around major U.S. tariff episodes

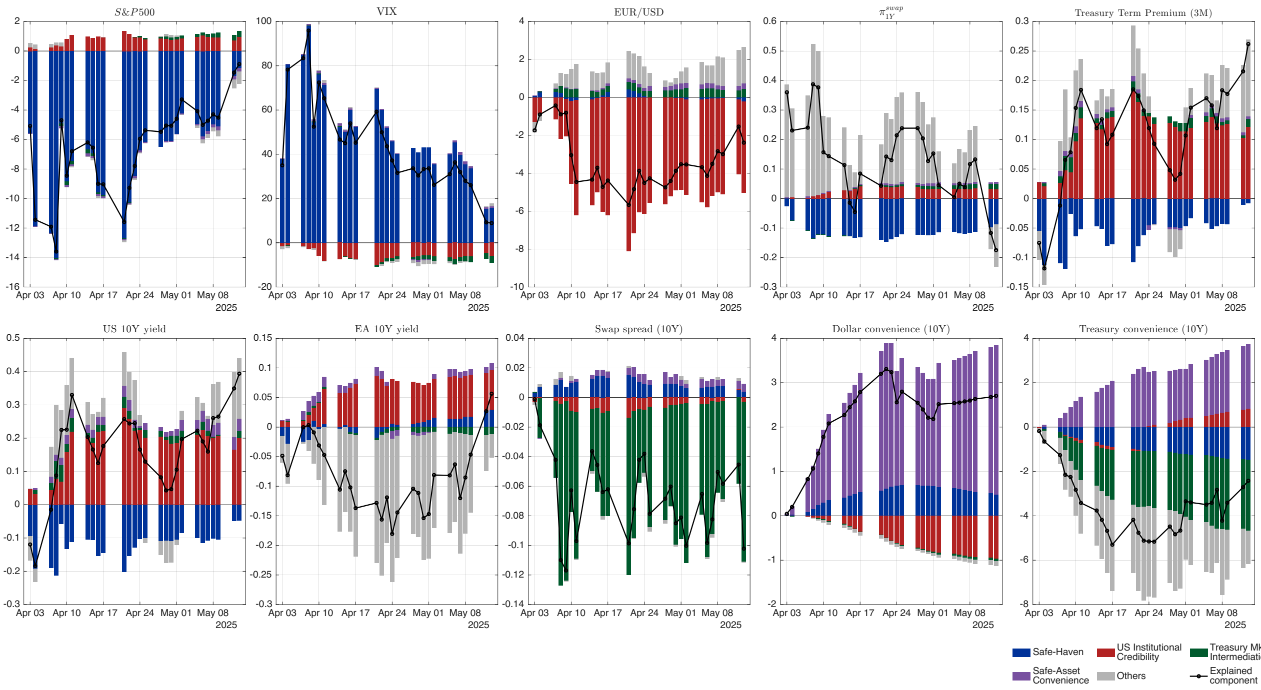

(a) April 2025 Tariff Announcement

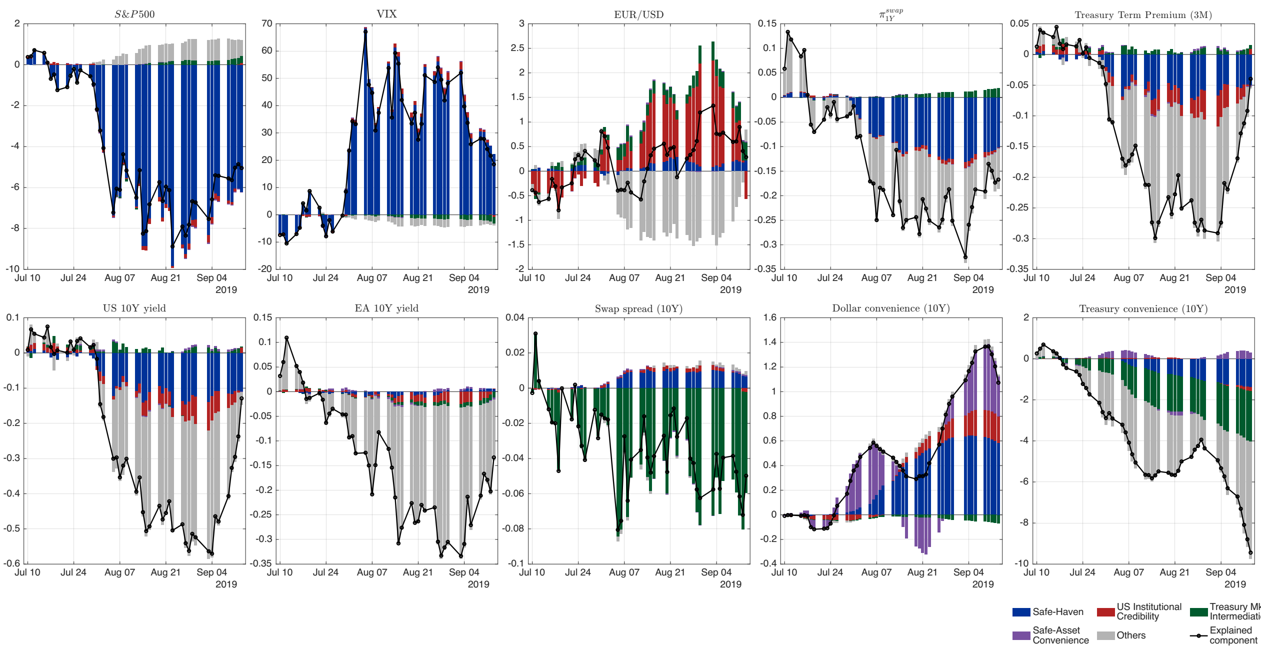

(b) August 2019 tariff escalation

Notes: Panel (a): historical decomposition for the April 2025 tariff window (2 April–14 May 2025). Panel (b): historical decomposition for the August 2019 tariff-escalation episode (9 July–15 September 2019). Stacked bars show the cumulative contributions of grouped statistically identified structural shocks; the black line is the explained component (deviation from the deterministic component). *Safe-Haven shock* = shocks 1–2; *U.S. Institutional Credibility shock* = shock 3; *Treasury Market Intermediation shock* = shock 8; *Safe-Asset Convenience shock* = shock 9; other shocks = shocks 4–7 and 10.

of a weaker dollar, higher long-term U.S. Treasury yields, and lower euro-area long-term yields cannot be interpreted as the propagation of a single tariff-announcement shock.

The third result concerns the distinct forces driving Dollar Convenience and Treasury Convenience. The decomposition shows that the two measures are driven by different structural shocks. Dollar Convenience is shaped mainly by the *U.S. Institutional Credibility shock* and the *Safe-Asset Convenience shock*. Treasury Convenience, by contrast, is driven primarily by the *Treasury Market Intermediation shock*, which also accounts for the deterioration in swap spreads. This close comovement is consistent with the interpretation of Du et al. (2026) that declines in Treasury Convenience increasingly reflect disruptions to Treasury-market intermediation and dealer balance-sheet capacity rather than changes in the broader convenience value of dollar-denominated safe assets. It also accords with the mechanism emphasized by Kashyap et al. (2025), whereby tighter intermediary balance-sheet constraints and reduced arbitrage capacity impair Treasury-market functioning.

Panel (b) of Figure 4 reports the corresponding decomposition for the August 2019 tariff escalation. The earlier episode is explained to a greater extent by the *Safe-Haven shock*, while the contributions of the *U.S. Institutional Credibility shock* and the *Treasury Market Intermediation shock* are more limited. Notably, the *Safe-Haven shock* also accounts for part, although not all, of the decline in the term premium and long-term U.S. Treasury yields. The comparison suggests that the 2025 episode did not generate entirely new mechanisms. Rather, it amplified forces that were already present during the 2019 tariff episode. Whereas the earlier episode remained largely consistent with a conventional safe-haven interpretation, the 2025 episode reflects the interaction of distinct shocks affecting confidence in U.S. institutions, Treasury-market intermediation, and the convenience value attached to dollar-denominated safe assets.

These findings complement the event-targeted VAR of Pinter et al. (2025). Their orthogonalised tariff-announcement shock explains much of the behaviour of equity prices, implied volatility, commodity prices, and short-term inflation expectations, while the persistent depreciation of the dollar and the behaviour of government bond yields are attributed to other orthogonal shocks. Our decomposition reaches a similar conclusion regarding the limits of a single tariff-announcement disturbance but goes one step further by identifying these additional disturbances as the *U.S. Institutional Credibility shock*, the *Treasury Market Intermediation shock*, and the *Safe-Asset Convenience shock*.

4 Conclusion

This paper studies the financial-market transmission of the April 2025 U.S. tariff announcements, with a particular focus on the unusual combination of dollar depreciation and rising long-term U.S. Treasury yields. Departing from event-based identification strategies that anchor the analysis on a single announcement shock, we adopt a statistical identification approach that exploits time variation in second moments and excess kurtosis to recover the contemporaneous transmission of shocks across financial markets. This framework is particularly well suited to the April 2025 episode, which was characterised by large, heterogeneous disturbances, pronounced volatility shifts, and rapidly changing market conditions.

Our results show that the April 2025 tariff episode cannot be understood as the propagation of a single tariff-announcement or safe-haven shock. Instead, the impulse responses and historical decomposition reveal that different components of the financial-market response were driven by distinct orthogonal macro-financial shocks. Conventional safe-haven forces explain the initial broad risk-off response, particularly the behaviour of equity markets. However, they cannot account for the subsequent combination of dollar depreciation and rising long-term Treasury yields, which departs both from standard flight-to-safety dynamics and from canonical tariff-transmission mechanisms.

Instead, the evidence points to distinct shocks associated with conventional safe-haven demand, the *U.S. Institutional Credibility shock*, and the *Treasury Market Intermediation shock*. The historical decomposition shows that these shocks dominate different financial variables rather than propagating uniformly across markets. This distinction reconciles the apparently contradictory behaviour of equity prices, exchange rates, and fixed-income markets following the tariff announcement. It also supports the view that Dollar Convenience and Treasury Convenience capture distinct dimensions of U.S. international privilege rather than a single underlying safe-haven factor.

A key implication of these findings is that exchange-rate dynamics following major trade-policy announcements need not reflect the propagation of a single underlying economic force. Even when the initial announcement triggers a conventional risk-off response, subsequent price adjustments may be dominated by orthogonal macro-financial disturbances. More broadly, our results suggest that U.S. international privilege is best understood as comprising several distinct dimensions. Confidence in U.S. institutions, Treasury-market functioning, and the convenience value attached to dollar-denominated safe assets can evolve independently, making it essential to distinguish these mechanisms when interpreting periods of stress in the international monetary system.

References

Adrian, Tobias, Richard K. Crump and Emanuel Moench. (2013). "Pricing the term structure with linear regressions". *Journal of Financial Economics*, 110(1), pp. 110-138. https://doi.org/10.1016/j.jfineco.2013.04.009

Alessandria, George A., Jiaxiaomei Ding, Shafaat Y. Khan and Carter B. Mix. (2025). "The tariff tax cut: Tariffs as revenue". NBER Working Paper Series, 33784, National Bureau of Economic Research. https://doi.org/10.3386/w33784

Auclert, Adrien, Matthew Rognlie and Ludwig Straub. (2025). "The macroeconomics of tariff shocks". NBER Working Paper Series, 33726, National Bureau of Economic Research. https://doi.org/10.3386/w33726

Baumeister, Christiane, and James D. Hamilton. (2019). "Structural interpretation of vector autoregressions with incomplete identification: Revisiting the role of oil supply and demand shocks". *American Economic Review*, 109(5), pp. 1873-1910. https://doi.org/10.1257/aer.20151569

Bauwens, Luc, and Michel Lubrano. (1998). "Bayesian inference on GARCH models using the Gibbs sampler". *The Econometrics Journal*, 1(1), pp. C23-C46. https://doi.org/10.1111/1368-423X.11003

Bertsche, Dominik, and Robin Braun. (2022). "Identification of structural vector autoregressions by stochastic volatility". *Journal of Business & Economic Statistics*, 40(1), pp. 328-341. https://doi.org/10.1080/07350015.2020.1813588

Boyarchenko, Nina, Pooja Gupta, Nick Steele and Jacqueline Yen. (2018). "Negative swap spreads". *Economic Policy Review*, 24(2), pp. 1-14. https://www.newyorkfed.org/research/epr/2018/epr_2018_negative-swap-spreads_boyarchenko

Brunnermeier, Markus, Darius Palia, Karthik A. Sastry and Christopher A. Sims. (2021). "Feedbacks: Financial markets and economic activity". *American Economic Review*, 111(6), pp. 1845-1879. https://doi.org/10.1257/aer.20180733

Bruno, Valentina, and Hyun Song Shin. (2017). "Global dollar credit and carry trades: A firm-level analysis". *The Review of Financial Studies*, 30(3), pp. 703-749. https://doi.org/10.1093/rfs/hhw099

Carriero, Andrea, Todd E. Clark, Massimiliano Marcellino and Elmar Mertens. (2024). "Addressing COVID-19 outliers in BVARs with stochastic volatility". *The Review of Economics and Statistics*, 106(5), pp. 1403-1417. https://doi.org/10.1162/rest_a_01213

Cetorelli, Nicola, and Linda S. Goldberg. (2012). "Banking globalization and monetary transmission". *The Journal of Finance*, 67(5), pp. 1811-1843. https://doi.org/10.1111/j.1540-6261.2012.01773.x

Chan, Joshua C. C. (2024). "Chapter 3: BVARs and stochastic volatility". En Michael P. Clements y Ana Beatriz Galvão (eds.), *Handbook of Research Methods and Applications in Macroeconomic Forecasting*. Edward Elgar Publishing, pp. 43-67. https://doi.org/10.4337/9781035310050.00007

Chan, Joshua C. C. (2020). "Large bayesian VARs: A flexible kronecker error covariance structure". *Journal of Business & Economic Statistics*, 38(1), pp. 68-79. https://doi.org/10.1080/07350015.2018.1451336

Chan, Joshua C. C., and Cody Y. L. Hsiao. (2014). “Estimation of stochastic volatility models with heavy tails and serial dependence”. *Bayesian Inference in the Social Sciences*, pp. 155-176. https://doi.org/10.1002/9781118771051.ch6

Chan, Joshua C. C., Gary Koop and Xuewen Yu. (2024). “Large order-invariant Bayesian VARs with stochastic volatility”. *Journal of Business & Economic Statistics*, 42(2), pp. 825-837. https://doi.org/10.1080/07350015.2023.2252039

Chiu, Ching-Wai (Jeremy), Haroon Mumtaz and Gábor Pintér. (2017). “Forecasting with VAR models: Fat tails and stochastic volatility”. *International Journal of Forecasting*, 33(4), pp. 1124-1143. https://doi.org/https://doi.org/10.1016/j.ijforecast.2017.03.001

Clark, Todd E. (2011). “Real-time density forecasts from Bayesian vector autoregressions with stochastic volatility”. *Journal of Business & Economic Statistics*, 29(3), pp. 327-341. https://doi.org/10.1198/jbes.2010.09248

Del Negro, Marco, and Giorgio E. Primiceri. (2015). “Time varying structural vector autoregressions and monetary policy: A corrigendum”. *The Review of Economic Studies*, 82(4), pp. 1342-1345. https://doi.org/10.1093/restud/rdv024

Du, Wenxin, Joanne Im and Jesse Schreger. (2018a). “The U.S. Treasury Premium”. *Journal of International Economics*, 112, pp. 167-181. https://doi.org/10.1016/j.jinteco.2018.01.001

Du, Wenxin, Ritt Keerati and Jesse Schreger. (2026). “Decoupling Dollar and Treasury Privilege”. NBER Working Paper Series, 35000, National Bureau of Economic Research. https://doi.org/10.3386/w35000

Du, Wenxin, Alexander Tepper and Adrien Verdelhan. (2018b). “Deviations from covered interest rate parity”. *The Journal of Finance*, 73(3), pp. 915-957. https://doi.org/10.1111/jofi.12620

Frankovic, Ivan, and Sören Karau. (2026). “Political Pressure on the Fed - Is This Time Different?”. SSRN Working Paper, 6173431. https://doi.org/10.2139/ssrn.6173431

Furceri, Davide, Swarnali A. Hannan, Jonathan D. Ostry and Andrew K. Rose. (2018). “Macroeconomic consequences of tariffs”. NBER Working Paper Series, 25402, National Bureau of Economic Research. https://doi.org/10.3386/w25402

Georgiadis, Georgios, and Arnaud Mehl. (2015). “Trilemma, not dilemma: financial globalisation and monetary policy effectiveness”. Globalization and Monetary Policy Institute Working Paper, 222, Federal Reserve Bank of Dallas. https://doi.org/10.24149/gwp222

Georgiadis, Georgios, Gernot J. Müller and Ben Schumann. (2024). “Global risk and the dollar”. *Journal of Monetary Economics*, 144(103549). https://doi.org/10.1016/j.jmoneco.2024.01.002

Geweke, John, and Gianni Amisano. (2010). “Comparing and evaluating Bayesian predictive distributions of asset returns”. *International Journal of Forecasting*, 26(2), pp. 216-230. https://doi.org/10.1016/j.ijforecast.2009.10.007

Gopinath, Gita, Emine Boz, Camila Casas, Federico J. Díez, Pierre-Olivier Gourinchas and Mikkel Plagborg-Møller. (2020). “Dominant currency paradigm”. *American Economic Review*, 110(3), pp. 677-719. https://doi.org/10.1257/aer.20171201

Gopinath, Gita, and Jeremy C. Stein. (2021). “Banking, trade, and the making of a dominant currency”. *The Quarterly Journal of Economics,* 136(2), pp. 783-830. https://doi.org/10.1093/qje/qjaa036

Gourinchas, Pierre-Olivier, and Hélène Rey. (2007). “1 From world banker to world venture capitalist: U.S. external adjustment and the exorbitant privilege”. En Richard H. Clarida (ed.), *G7 current account imbalances: Sustainability and adjustment.* University of Chicago Press, pp. 11-66. https://doi.org/10.7208/chicago/9780226107288.003.0002

Gourinchas, Pierre-Olivier, and Hélène Rey. (2022). “Exorbitant privilege and exorbitant duty”. CEPR Discussion Paper, DP16944, Centre for Economic Policy Research. https://cepr.org/publications/dp16944

Habib, Maurizio M., and Livio Stracca. (2012). “Getting beyond carry trade: What makes a safe haven currency?”. *Journal of International Economics,* 87(1), pp. 50-64. https://doi.org/10.1016/j.jinteco.2011.12.005

Hartley, Jonathan, and Alessandro Rebucci. (2025). *Tariffs, the dollar, and equities: High-frequency evidence from the liberation day announcement.* VoxEU – CEPR’s policy portal. https://cepr.org/voxeu/columns/tariffs-dollar-and-equities-high-frequency-evidence-liberation-day-announcement

Hossfeld, Oliver, and Ronald MacDonald. (2015). “Carry funding and safe haven currencies: A threshold regression approach”. *Journal of International Money and Finance,* 59, pp. 185-202. https://doi.org/10.1016/j.jimonfin.2015.07.005

Ignatenko, Anna, Ahmad Lashkaripour, Luca Macedoni and Ina Simonovska. (2025). “Making America great again? The economic impacts of Liberation Day tariffs”. *Journal of International Economics,* 157(104138). https://doi.org/10.1016/j.jinteco.2025.104138

Ivashina, Victoria, David S. Scharfstein and Jeremy C. Stein. (2015). “Dollar funding and the lending behavior of global banks”. *The Quarterly Journal of Economics,* 130(3), pp. 1241-1281. https://doi.org/10.1093/qje/qjv017

Jarocinski, Marek. (2024). “Estimating the Fed’s unconventional policy shocks”. *Journal of Monetary Economics,* 144(103548). https://doi.org/10.1016/j.jmoneco.2024.01.001

Jeanne, Olivier, and Jeongwon Son John. (2024). “To what extent are tariffs offset by exchange rates?”. *Journal of International Money and Finance,* 142(103015). https://doi.org/10.1016/j.jimonfin.2024.103015

Jiang, Zhengyang, Arvind Krishnamurthy and Hanno Lustig. (2018). “Foreign safe asset demand for U.S. Treasurys and the dollar”. *AEA Papers and Proceedings,* 108, pp. 537-541. https://doi.org/10.1257/pandp.20181064

Jiang, Zhengyang, Arvind Krishnamurthy and Hanno Lustig. (2021). “Foreign safe asset demand and the dollar exchange rate”. *The Journal of Finance,* 76(3), pp. 1049-1089. https://doi.org/10.1111/jofi.13003

Jiang, Zhengyang, Arvind Krishnamurthy and Hanno Lustig. (2024a). “Dollar safety and the global financial cycle”. *The Review of economic studies,* 91(5), pp. 2878-2915. https://doi.org/10.1093/restud/rdad108

Jiang, Zhengyang, Robert J. Richmond and Tony Zhang. (2024b). "A portfolio approach to global imbalances". *The Journal of Finance*, 79(3), pp. 2025-2076. https://doi.org/10.1111/jofi.13333

Kalemli-Özcan, Şebnem, Can Soylu and Muhammed A. Yildirim. (2025). "Global networks, monetary policy and trade". NBER Working Paper Series, 33686, National Bureau of Economic Research. https://doi.org/10.3386/w33686

Känzig, Diego R. (2021). "The macroeconomic effects of oil supply news: Evidence from OPEC announcements". *American Economic Review*, 111(4), pp. 1092-1125. https://doi.org/10.1257/aer.20190964

Kashyap, Anil K., Jeremy C. Stein, Jonathan L. Wallen and Joshua Younger. (2025). "Treasury market dysfunction and the role of the central bank". *Brookings Papers on Economic Activity*, Spring 2025. https://doi.org/10.1353/eca.2025.a978549

Kim, Sangjoon, Neil Shephard and Siddhartha Chib. (1998). "Stochastic volatility: Likelihood inference and comparison with ARCH models". *The Review of Economic Studies*, 65(3), pp. 361-393. https://doi.org/10.1111/1467-937X.00050

Kociecki, Andrzej, Christian Matthes and Michele Piffer. (2025). "A non-Gaussian GDP anatomy". *Working Paper*. https://cm1518.github.io/files/Non_Gaussian_Business_Cycle_Anatomy.pdf

Krishnamurthy, Arvind, and Hanno N. Lustig. (2019). *Mind the gap in sovereign debt markets: The U.S. Treasury basis and the dollar risk factor*. Challenges for Monetary Policy - Jackson Hole Economic Policy Symposium - Federal Reserve Bank of Kansas City, August 22-24, Jackson Hole, Wyoming, pp. 445-507. https://www.kansascityfed.org/Jackson%20Hole/documents/6963/Krishnamurthy_JH2019.pdf

Lanne, Markku, Mika Meitz and Pentti Saikkonen. (2017). "Identification and estimation of non-Gaussian structural vector autoregressions". *Journal of Econometrics*, 196(2), pp. 288-304. https://doi.org/10.1016/j.jeconom.2016.06.002

Lütkepohl, Helmut, and Thore Schlaak. (2018). "Choosing between different time-varying volatility models for structural vector autoregressive analysis". *Oxford Bulletin of Economics and Statistics*, 80(4), pp. 715-735. https://doi.org/10.1111/obes.12238

Maggiori, Matteo, Brent Neiman and Jesse Schreger. (2020). "International currencies and capital allocation". *Journal of Political Economy*, 128(6), pp. 2019-2066. https://doi.org/10.1086/705688

Ni, Shawn, and Dongchu Sun. (2005). "Bayesian estimates for vector autoregressive models". *Journal of Business & Economic Statistics*, 23(1), pp. 105-117. https://doi.org/10.1198/073500104000000622

Ostry, Daniel, Simon Lloyd and Giancarlo Corsetti. (2025). "Trading blows: The exchange-rate response to tariffs and retaliations". Staff Working Paper, 1139, Bank of England. https://www.bankofengland.co.uk/working-paper/2025/trading-blows-the-exchange-rate-response-to-tariffs-and-retaliations

Pinter, Gabor, Frank Smets and Semih Uslu. (2025). "Market whiplash after the 2025 tariff shock: An event-targeted VAR approach". Research Paper, Johns Hopkins Carey Business School. Forthcoming. https://doi.org/10.2139/ssrn.5303690

Poworoznek, Evan, Niccolo Anceschi, Federico Ferrari and David Dunson. (2021). “Efficiently resolving rotational ambiguity in Bayesian matrix sampling with matching”. arXiv, 2107. 13783 [Preprint]. https://arxiv.org/abs/2107.13783

Rey, Hélène. (2015). “Dilemma not trilemma: the global financial cycle and monetary policy independence”. NBER Worling Paper Series, 21162, National Bureau of Economic Research. https://doi.org/10.3386/w21162

Rigobon, Roberto. (2003). “Identification through heteroskedasticity”. *The Review of Economics and Statistics*, 85(4), pp. 777-792. https://doi.org/10.1162/003465303772815727

Ritter, Christian, and Martin A. Tanner. (1992). “Facilitating the Gibbs sampler: the Gibbs stopper and the griddy-Gibbs sampler”. *Journal of the American Statistical Association*, 87(419), pp. 861-868. https://doi.org/10.1080/01621459.1992.10475289

Rodríguez-Clare, Andrés, Mauricio Ulate and Jose P. Vasquez. (2025). “The 2025 trade war: Dynamic impacts across U.S. states and the global economy”. NBER Working Paper Series, 33792, National Bureau of Economic Research.https://doi.org/10.3386/w33792

Shin, Hyun Song. (2012). “Global banking glut and loan risk premium”. *IMF Economic Review*, 60(2), pp. 155-192. https://doi.org/10.1057/imfer.2012.6

Sims, Christopher A. (2021). “SVAR identification through heteroskedasticity with misspecified regimes”. Discussion paper, Princeton University. http://sims.princeton.edu/yftp/bpss/IDHmsspcfdRgms.pdf

Villani, Mattias. (2009). “Steady-state priors for vector autoregressions”. *Journal of Applied Econometrics*, 24(4), pp. 630-650. https://doi.org/10.1002/jae.1065

Waggoner, Daniel F., and Tao Zha. (1999). “Conditional forecasts in dynamic multivariate models”. *The Review of Economics and Statistics*, 81(4), pp. 639-651. https://doi.org/10.1162/003465399558508

Waggoner, Daniel F., and Tao Zha. (2003). “A Gibbs sampler for structural vector autoregressions”. *Journal of Economic Dynamics and Control*, 28(2), pp. 349-366. https://doi.org/10.1016/S0165-1889(02)00168-9

Appendices

A Model details

The model is given as follows:

$$y_t = b_0 + B_1 y_{t-1} + \ldots + B_p y_{t-p} + A^{-1}\epsilon_t \tag{A.1}$$

$$\epsilon_t|\omega_t \sim \mathcal{N}(0,\Omega_t), \quad \Omega_t = diag(\omega_{1,t}e^{h_{1,t}},\ldots,\omega_{N,t}e^{h_{N,t}}) \tag{A.2}$$

$$\omega_{i,t} \sim \mathcal{IG}\left(\frac{\nu_i}{2},\frac{\nu_i}{2}\right), \quad \nu_i > 0 \tag{A.3}$$

$$h_{i,t} = \rho_i h_{i,t-1} + v_{i,t}, \quad |\rho_i| < 1, \quad v_{i,t} \sim \mathcal{N}(0,\sigma_i^2) \tag{A.4}$$

$$h_{i,1} \sim \mathcal{N}\left(0,\frac{\sigma_i^2}{1-\rho_i^2}\right) \tag{A.5}$$

where y_t is an $N \times 1$ vector of endogenous variables and ϵ_t contains structural shocks that are independent across equations and time. The structural matrix A is assumed to be invertible but otherwise unrestricted.

A.1 Likelihood function

The likelihood is easy to derive as the data are conditionally Gaussian. First, denote the collection of model parameters as Θ, including the log-volatility processes and latent scaling factors $\omega_{i,t}$. Next, write a generic observation at time t as:

$$y_t = B'x_t + A^{-1}\epsilon_t \tag{A.6}$$

$$x_t = [y'_{t-1},\ldots,y'_{t-p},1]' \tag{A.7}$$

Stacking the transposed model equations below each other into the $T \times N$ matrix Y yields:

$$Y = XB + E(A^{-1})' \tag{A.8}$$

where the matrix X has the vectors x'_t as its rows. We then have the vectorized model as:

$$\text{vec}(Y) \equiv y = \tilde{X}\beta + (A^{-1}\otimes I_T)\epsilon \tag{A.9}$$

$$\tilde{X} \equiv (I_N \otimes X) \tag{A.10}$$

$$\epsilon \sim \mathcal{N}(0,\Omega) \tag{A.11}$$

$$\Omega = \text{diag}(\omega_{1,1}e^{h_{1,1}},\ldots,\omega_{1,T}e^{h_{1,T}},\ldots,\omega_{N,1}e^{h_{N,1}},\ldots,\omega_{N,T}e^{h_{N,T}}) \tag{A.12}$$

It then follows that the likelihood function is given by:

$$p(y|\theta) \propto |\det(A)|^T \det(\Omega)^{-1/2} e^{-\frac{1}{2}(y-\tilde{X}\beta)'\tilde{\Omega}^{-1}(y-\tilde{X}\beta)} \tag{A.13}$$

where $\tilde{\Omega} = (A^{-1} \otimes I_T)\Omega(A^{-1} \otimes I_T)'$.

A.2 Prior distributions

The prior on the impact matrix is flat which we implement via a Normal distribution with zero precision, i.e. we assume:

$$\alpha \sim \mathcal{N}(\alpha_0, K_\alpha^{-1}) \tag{A.14}$$

and set $\alpha_0 = 0$ and $K_\alpha = 0$. One could set an informative prior here as in Brunnermeier et al. (2021) which would also help mitigate the rotational ambiguity present in this model, but we refrain from doing so because there is no clear guidance as to how to specify the elements of this matrix, and we wish to impose as little identifying assumptions on the model as possible.

Next, we assume a Normal distribution for the VAR parameters:

$$\beta \sim \mathcal{N}(\beta_0, V_\beta) \tag{A.15}$$

which is parameterized in the conventional Minnesota fashion. The elements of β_0 are set equal to zero, except for the first autoregressive coefficients in each equation that are set to one for variables in log-levels and zero for variables expressed as interest rates and spreads. The elements of V_β are set as follows. For coefficients belonging to the lags of the variable in equation i we set the prior variance equal to $\left(\lambda_1 k^{-\lambda_3} s_i\right)^2$. For coefficients belonging to another variable j we set the prior variance equal to $\left(\lambda_1 \lambda_2 k^{-\lambda_3} \frac{s_i}{s_j}\right)^2$. The terms s_i^2 are obtained as residual variances from univariate AR(p) models. The overall shrinkage parameter λ_1 is set to 0.2, the cross-variable shrinkage parameter λ_2 is set to 0.5, and the lag-decay parameter λ_3 equals 1. Lastly, for the constant term in equation i we set the prior variance equal to $100 s_i^2$.

The prior on the degrees of freedom controls the prior degree of non-Gaussianity and we use a truncated Gamma distribution:

$$\nu_i \sim \mathcal{G}(s_\nu, \delta_\nu) \mathbb{1}_{\nu_i \in [\underline{\nu}, \overline{\nu}]} \tag{A.16}$$

We tilt the odds towards the Gaussian model by setting $s_\nu = 4$ and $\delta_\nu = 5$, implying a mean of 20 and variance 100 before truncation. The lower bound is set to $\underline{\nu} = 0.1$ to avoid the singularity problems occurring for very small degrees of freedom outlined in Bauwens and Lubrano (1998), while the upper bound $\overline{\nu} = 50$ ensures that we do not assign too much prior weight to the Gaussian model.

Lastly, regarding the stochastic volatility parameters of the model we set the following prior distributions:

$$\rho_i \sim \mathcal{N}(\rho_0, V_\rho)\mathbb{1}_{|\rho_i|<1} \tag{A.17}$$

$$\sigma_i^2 \sim \mathcal{IG}\left(\frac{s_\sigma}{2}, \frac{\delta_\sigma}{2}\right) \tag{A.18}$$

where the hyperparameters are set to $\rho_0 = 0.95$, $V_\rho = 0.05^2$, $s_\sigma = 6$, and $\delta_\sigma = 0.2$.

A.3 MCMC algorithm

To help with the exposition of the MCMC algorithm we first write out the necessary terms of the posterior density to be sampled from. For this, multiply the likelihood function with the prior, assuming prior independence across the parameter blocks, which yields:

$$\begin{aligned} p(\Theta|y) \propto & \underbrace{|\det(A)|^T \det(\Omega)^{-1/2} e^{-\frac{1}{2}(y-\tilde{X}\beta)'\tilde{\Omega}^{-1}(y-\tilde{X}\beta)}}_{p(y|\Theta)} \\ & \cdot \underbrace{e^{-\frac{1}{2}(\beta-\beta_0)'V_\beta^{-1}(\beta-\beta_0)}}_{p(\beta)} \\ & \cdot \underbrace{\prod_i \left(\frac{\sigma_i^2}{1-\rho_i^2}\right)^{-1/2} e^{-\frac{(1-\rho_i^2)h_{i,1}^2}{2\sigma_i^2}} (\sigma_i^2)^{-\frac{T-1}{2}} e^{-\frac{1}{2\sigma_i^2}\sum_{t=2}^T (h_{i,t}-\rho_i h_{i,t-1})^2}}_{p(h|\rho,\sigma^2)} \\ & \cdot \underbrace{\prod_i e^{-\frac{1}{2}(\rho_i-\rho_0)'V_\rho^{-1}(\rho_i-\rho_0)} \mathbb{1}_{\rho_i \in(-1,1)} \cdot (\sigma_i^2)^{-\left(\frac{s_\sigma}{2}+1\right)} e^{-\frac{\delta_\sigma}{2\sigma_i^2}}}_{p(\rho,\sigma^2)} \\ & \cdot \underbrace{\prod_i \Gamma\left(\frac{\nu_i}{2}\right)^{-T} \left(\frac{\nu_i}{2}\right)^{T\nu_i/2} \prod_t \omega_{i,t}^{-\left(\frac{\nu_i}{2}+1\right)} e^{-\frac{\nu_i-2}{2\omega_{i,t}}}}_{p(\omega|\nu)} \\ & \cdot \underbrace{\prod_i \nu_i^{s_\nu-1} e^{-\frac{\nu_i}{\delta_\nu}} \mathbb{1}_{\nu_i \in[\underline{\nu},\overline{\nu}]}}_{p(\nu)} \end{aligned} \tag{A.19}$$

Recall that we set a flat prior on A so that its prior density does not show up. An informative prior can be added, as long as it is Gaussian and the rows of A are a priori independent. The above density is not tractable and MCMC methods are used to draw samples from it. In the following we write all distributions conditional on the data y and the parameter vector θ, where, to avoid notational clutter, it is understood that the respective parameter to be sampled is not part of the conditioning set.

Step 1. Draw from $p(\alpha|y,\theta) = p(\alpha|y,\beta,\omega,\nu,h)$.
To sample from this density we follow directly the algorithm outlined in Chan et al. (2024) to sample each row of A conditional on the other rows, which is an application of results in Waggoner and Zha (2003) and Villani (2009). To this end, write the model for row i as:

$$(Y - XB)a_i = E_i \tag{A.20}$$
$$E_i \sim \mathcal{N}(0, \Omega_i) \tag{A.21}$$
$$\Omega_i = \operatorname{diag}(\omega_{i,1}e^{h_{i,1}}, \ldots, \omega_{i,T}e^{h_{i,T}}) \tag{A.22}$$

The authors then show that one can produce a draw for α_i by drawing the elements of this vector from:

$$\alpha_i(1) \sim \mathcal{AN}\left(\phi_1, T^{-1}\right) \tag{A.23}$$
$$\alpha_i(j) \sim \mathcal{N}\left(\phi_j, T^{-1}\right), \quad j = 2, \ldots, N \tag{A.24}$$

where, for each element $j = 1, \ldots, N$, the means of these distributions are given by:

$$\phi_j = \hat{a}_i' C_j v_j \tag{A.25}$$
$$\hat{a}_i = \bar{K}_{\alpha_i}^{-1} K_{\alpha_i} \alpha_{0,i} \tag{A.26}$$
$$\bar{K}_\alpha = K_{\alpha_i} + (Y - XB)'\Omega_i^{-1}(Y - XB) \tag{A.27}$$
$$C_i C_i' = T^{-1}\bar{K}_{\alpha_i} \tag{A.28}$$
$$v = (v_1, v_2, \ldots, v_N) \tag{A.29}$$
$$v_1 = C_i^{-1}(A'_{-i})^{\perp}/||C_i^{-1}(A'_{-i})^{\perp}|| \tag{A.30}$$
$$(v_2, \ldots, v_N) = v_1^{\perp} \tag{A.31}$$

and $x^{\perp}$ denotes the orthogonal complement of x, while A_{-i} is the matrix A with its i-th column deleted. Note that (A.28) is meant as a computational instruction that states to compute C_i as the lower triangular Cholesky factorization of $T^{-1}\bar{K}_{\alpha_i}$. How to draw from the absolute normal distribution is outlined in Villani (2009).

Step 2. Draw from $p(\beta|y,\theta) = p(\beta|y,\alpha,\omega,h)$.
From standard arguments then follows the usual Gaussian conditional posterior for β:

$$\beta|y,\theta \sim \mathcal{N}(\bar{\beta},\bar{V}_\beta) \tag{A.32}$$
$$\bar{V}_\beta = \left(V_\beta^{-1} + (A\otimes X)'\Omega^{-1}(A\otimes X)\right)^{-1} \tag{A.33}$$
$$\bar{\beta} = \bar{V}_\beta\left(V_\beta^{-1}\beta_0 + (A\otimes X)'\Omega^{-1}\operatorname{vec}(YA')\right) \tag{A.34}$$

In practice, we do not compute the inverse matrix, but rather work with the precision matrix, which makes for more efficient sampling (see Chan (2020) for implementation details).

Step 3. Draw from $p(\omega|y,\theta) = \prod_t\prod_i p(\omega_{i,t}|y,\alpha,\beta,h_i,\nu_i)$.
We first purge the structural shocks of the stochastic volatility parameters via $E = ((Y-XB)A')\odot O^{-1/2}$, where the entries of the $T\times N$ matrix O are $e^{h_{i,t}}$, and $\odot$ denotes the Hadamard product (i.e. element-wise multiplication). Then, with these shocks in hand it is easy to verify that the conditional posterior distributions are given by:

$$\omega_{i,t}|y,\theta \sim \mathcal{IG}\left(\frac{\nu_i+1}{2},\frac{\nu_i+e_{i,t}^2}{2}\right) \tag{A.35}$$

Step 4. Draw from $p(\nu|y,\theta) = \prod_i p(\nu_i|\omega_i)$.
As for the previous step the degrees of freedom parameters occur in the expressions for the structural errors of equation i, the prior densities for $\omega_{i,t}$, and in their own priors. Hence we have:

$$p(\nu_i|y,\theta) \propto p(\nu_i)\Gamma\left(\frac{\nu_i}{2}\right)^{-T}\left(\frac{\nu_i-2}{2}\right)^{\frac{T\nu_i}{2}}\prod_t \omega_{i,t}^{-\frac{\nu_i}{2}}e^{-\frac{1}{\omega_{i,t}}\frac{\nu_i-2}{2}} \tag{A.36}$$

where $p(\nu_i)$ is the prior density given above. This density is again non-standard and again we draw from it using a Griddy-Gibbs sampling step.

Step 5. Draw from $p(\sigma^2|y,\theta) = \prod_i p(\sigma_i^2|h_i,\rho_i)$.

This step is standard, as the conditional posterior takes the simple form:

$$\sigma_i^2|y,\theta \sim \mathcal{IG}\left(\frac{\alpha_0+T}{2}, \frac{S_0+(1-\rho_i^2)h_{i,1}^2+\sum_{t=2}^{T}(h_{i,t}-\rho_i h_{i,t-1})^2}{2}\right) \tag{A.37}$$

Step 6. Draw from $p(\rho|y,\theta)=\prod_i p(\rho_i|h_i,\sigma_i^2)$.
From the prior distribution and the log-volatility process it is easy to derive that the conditional posterior is proportional to the following density:

$$p(\rho_i|h_i,\sigma_i^2) \propto p(\rho_i)g(\rho_i)e^{-\frac{1}{2\sigma_i^2}\sum_{t=2}^{T}(h_{i,t}-\rho_i h_{i,t-1})^2} \tag{A.38}$$

$$g(\rho_i)=(1-\rho_i^2)^{1/2}e^{-\frac{1}{2\sigma_i^2}(1-\rho_i^2)h_{i,1}^2} \tag{A.39}$$

This density is non-standard and we draw from it using a Griddy-Gibbs step.

Step 7. Draw from $p(h|y,\theta)=\prod_i p(h_i|y,A,\beta,\rho_i,\sigma_i^2,\gamma_i,\nu_i,\omega_i)$.
We use the auxiliary mixture sampler from Kim et al. (1998) to sample from this density. As the data in this sampling step for equation i we use column i of $E=((Y-XB)A')\odot O^{-1/2}$, where this time the entries of the matrix O are $\omega_{i,t}$. The implementation of the sampling step is well explained in Chan and Hsiao (2014), and we refer to both references for further details on the implementation. We only note that it is important to draw the mixture indicators before the log-volatilities in order to sample from the correct conditional posterior (see Del Negro and Primiceri (2015) and Chan (2024)).

A.4 Resolving rotational ambiguity

The rotational ambiguity in the model arises because one can always define a signed permutation matrix P_s such that the following reduced form error terms are observationally equivalent:

$$A^{-1}\epsilon_t = A^{-1}P_sP_s'\epsilon_t \equiv \tilde{A}^{-1}\tilde{\epsilon}_t \tag{A.40}$$

Note that the rotation matrices in models such as ours are restricted to signed column permutations. In contrast, in the usual Gaussian VAR model any conceivable orthogonal matrix is allowed for, making the identification issue more prevalent there (see also the discussions in Lanne et al. (2017) and Bertsche and Braun (2022) and the references therein). While non-Gaussianity can provide additional identifying information through higher-order moments, identification in our framework primarily relies on variation in second moments. Resolving the permutation ambiguity merely requires mapping the posterior draws consistently to the neighborhood of one arbitrarily chosen posterior mode. Intuitively, imagine a simple supply-demand setup with two structural shocks that is statistically identified, and that we have two draws for the impact matrix:

$$A_1^{-1} = \begin{pmatrix} 0.8 & 0.5 \\ 1.2 & -0.8 \end{pmatrix}, \quad A_2^{-1} = \begin{pmatrix} -0.4 & -0.5 \\ 0.4 & -0.8 \end{pmatrix} \tag{A.41}$$

Clearly, both matrices contain the same information about the effects of the shocks, one need only reorder the columns and switch the signs of the second matrix. This illustrates that the permutation issue has no impact on identification. It needs to be resolved, however, because in summary statistics across a sample of raw posterior draws, the opposing signs and column switches will cancel out and mask the economic content of the shocks. To do so, we use the approaches from Poworoznek et al. (2021) and Kociecki et al. (2025). Namely, given a MCMC sequence of draws for the impact matrix $D_{(m)} \equiv A_{(m)}^{-1}$ for $m = 1, \ldots, M$, we wish to find sign-permutations for each draw that minimize the squared Frobenius norm between the draws and some reference matrix $\hat{D} \equiv \hat{A}^{-1}$:

$$\min_{\{P_{s,(m)}\}} \sum_{m=1}^{M} ||D_{(m)} P_{s,(m)} - \hat{D}||_{\hat{A}}^2 = \min_{\{P_{s,(m)}\}} \sum_{m=1}^{M} \operatorname{tr}\left((D_{(m)} P_{s,(m)} - \hat{D})' \hat{A}' \hat{A} (D_{(m)} P_{s,(m)} - \hat{D}) \right) \tag{A.42}$$

Clearly, this is a minimization problem for each draw individually. Let us denote by tr_m the trace term for draw m. Expanding out this term gives

$$\begin{aligned} \operatorname{tr}_m &= \operatorname{tr}\left(P_{s,(m)}' D_{(m)}' \hat{A}' \hat{A} D_{(m)} P_{s,(m)} \right) - 2 \operatorname{tr}\left(\hat{D}' \hat{A}' \hat{A} D_{(m)} P_{s,(m)} \right) + \operatorname{tr}\left(\hat{D}' \hat{A}' \hat{A} \hat{D} \right) && \text{(A.43)} \\ &= \operatorname{tr}\left(D_{(m)}' \hat{A}' \hat{A} D_{(m)} \right) - 2 \operatorname{tr}\left(\hat{A} D_{(m)} P_{s,(m)} \right) + N && \text{(A.44)} \end{aligned}$$

Hence, we only need to consider the middle term of the last expression as the other terms are unaffected by the choice of signed permutation matrix. This is the approach proposed by Kociecki et al. (2025), and they show that one can equivalently solve the following modified problem:

$$\max_{P_{(m)}} \operatorname{tr}\left(|\hat{A} D_{(m)}| P_{(m)} \right) \tag{A.45}$$

where the absolute value is taken element-wise. Note here that thanks to the absolute value, the solution is simply a permutation matrix and the solution can be found easily using the built-in MATLAB function 'matchpairs'. For the algorithm we set the cost of an unmatched pair to zero with the maximization option of the function. We depart from Kociecki et al. (2025) in that we do not use the maximum likelihood estimator of A, but instead follow Poworoznek et al. (2021) and choose the sampled impact matrix with median condition number. Specifically, for the raw MCMC draws we first compute the condition number of each impact matrix. Second, we find the impact matrix with minimum Euclidean distance of its condition number to the median condition number, and take its inverse to obtain $\hat{A}$.

A.5 Implementation of the Griddy-Gibbs sampling step

In the above we draw some parameters using discrete approximations to the true conditional posteriors. Here we describe the general algorithm based on the exposition in Ritter and Tanner (1992), assuming that the generic density in question, $p(x)$, is univariate and its support is bounded, i.e. $x \in [\underline{x}, \overline{x}]$ where the bounds are finite. The integrating constant of the density does not need to be known. The random draw generation then proceeds as follows. First, create an ordered grid x_k of K points. In our application we use 500 grid points. One can space these points more densely in regions of the target density with high mass if this information is known. Next, evaluate the log of the target density at each grid point, giving $l_k \equiv \log(p(x_k))$ and record the largest value $l^M = \max_k(l_k)$. Then, adjust the probabilities via $\tilde{l}_k = l_k - l^M$ and calculate the grid point probabilities p_k as:

$$p_k = e^{\tilde{l}_k - \log\left(\sum_k e^{\tilde{l}_k}\right)} \tag{A.46}$$

This "LogSumExp" trick is a numerically stable way to calculate the probabilities, and one can verify that $p_k \geq 0 \ \forall k$ and $\sum_k p_k = 1$. Next, cumulate these probabilities to obtain an approximate CDF, denoted F. To produce a draw from this distribution, draw a uniform number $u \in [F_1, F_K]$ and locate the grid points x_j and x_{j+1} such that $u \in [F_j, F_{j+1}]$. Lastly, use a linear approximation of the CDF between these grid points and invert this linear function to find the final draw as:

$$x^* = x_j + \frac{u - F_j}{F_{j+1} - F_j}(x_{j+1} - x_j) \tag{A.47}$$

B Monte Carlo Simulation

In empirical applications, the true variance process is rarely known a priori. Different specifications capture different aspects of financial volatility: stochastic volatility models track persistent, low-frequency shifts in second moments, while fat-tailed distributions accommodate occasional extreme realisations through excess kurtosis, and combined specifications allow both features to coexist. The relevant question is therefore not only which specification fits best in-sample, but whether structural inference remains reliable when the variance process is misspecified. If the identification of the structural impact matrix depends sensitively on the exact parametrization of the variance dynamics, empirical conclusions could be fragile to routine modelling choices. If instead structural inference is robust across a range of variance specifications, the approach retains its validity even when the true volatility process is unknown.

To address these questions, we conduct a Monte Carlo simulation with two complementary objectives. First, we evaluate whether alternative variance specifications lead to materially different predictive performance when the true variance process is unknown. Second, we assess whether structural impulse responses can still be recovered accurately under variance misspecification. The Monte Carlo simulation therefore distinguishes predictive performance from structural identification and allows us to evaluate the robustness of the proposed identification strategy across alternative volatility environments.

Early contributions such as Rigobon (2003) and Ni and Sun (2005) introduced multivariate models with t-distributed structural shocks, highlighting the role of heavy tails in structural inference. More recently, Bertsche and Braun (2022) show that stochastic volatility can be exploited as an identification device in SVARs and demonstrate that the approach performs well even under variance misspecification. Chiu et al. (2017) show that combining low-frequency stochastic volatility with high-frequency fat-tailed shocks improves empirical fit, and Carriero et al. (2024) document that outlier-augmented stochastic volatility provides more stable density forecasts during extreme events. Motivated by this literature, the Monte Carlo simulation considers four data-generating processes that capture the main combinations of stochastic volatility and heavy-tailed innovations relevant to our model.

In line with the notation introduced in Section 2, the Monte Carlo simulation keeps three objects fixed across all simulation designs: the reduced-form VAR coefficient matrix B, the structural impact matrix A^{-1}, and therefore the true structural impulse responses. Only the variance process governing the structural shocks differs across the data-generating processes. This simulation design isolates the effect of variance misspecification on structural inference: because the true impulse responses are identical in all simulation designs, any differences in IRF recovery across specifications can be attributed directly to how well each model captures the relevant identifying variation. In the implementation, data are generated from the three-variable VAR(1)

$$y_t \;=\; x_t B + A^{-1}\epsilon_t, \qquad x_t = [y'_{t-1},\, 1], \qquad \epsilon_t \sim (0, \Omega_t), \tag{B.48}$$

with kept sample length $T = 500$ after burn-in and IRFs computed over a horizon of 16 periods. The common coefficient matrix and impact matrix are

$$B \;=\; \begin{pmatrix} 0.60 & -0.10 & 0.05 \\ 0.35 & 0.70 & -0.05 \\ 0.10 & 0.05 & 0.65 \\ 0.00 & 0.00 & 0.00 \end{pmatrix}, \qquad A^{-1} \;=\; \begin{pmatrix} 0.58 & 0.59 & 0.56 \\ -0.71 & 0.00 & 0.69 \\ 0.41 & -0.84 & 0.40 \end{pmatrix}$$

so only the shock process differs across the four DGPs. The volatility structures are specified as follows.

1. **Stochastic volatility (SV)**

$$\begin{aligned} &\omega_{i,t} \equiv 1, \qquad \varepsilon_t \mid h_t \sim \mathcal{N}\big(0,\ \mathrm{diag}(e^{h_{1,t}}, \dots, e^{h_{N,t}})\big)\,, \\ &h_{i,t} = \rho_i\, h_{i,t-1} + v_{i,t}, \quad v_{i,t} \sim \mathcal{N}(0, \sigma_i^2). \end{aligned}$$

The persistence parameters and innovation variances are set to

$$\rho_i \;=\; 0.95, \qquad \sigma_i^2 \;=\; 0.05, \qquad i = 1, 2, 3.$$

2. **t-Distribution**

$$\begin{aligned} \omega_{i,t} = \frac{1}{g_{i,t}}, \qquad g_{i,t} \sim \Gamma\Big(\tfrac{\nu_i}{2}, \tfrac{2}{\nu_i}\Big)\,, \\ \varepsilon_t \mid \omega_t \sim \mathcal{N}\big(0,\ \mathrm{diag}(\omega_{1,t}, \dots, \omega_{N,t})\big)\,. \end{aligned}$$

The degrees of freedom are equation-specific and set to

$$\nu = (2.5,\ 3,\ 4).$$

3. **SV-t**

$$\omega_{i,t} = \frac{1}{g_{i,t}}, \qquad g_{i,t} \sim \Gamma\left(\tfrac{\nu_i}{2}, \tfrac{2}{\nu_i}\right), \qquad h_{i,t} = \rho_i\, h_{i,t-1} + v_{i,t},$$
$$\varepsilon_t \mid \omega_t, h_t \sim \mathcal{N}\big(0,\ \mathrm{diag}\big(\omega_{1,t}e^{h_{1,t}}, \ldots, \omega_{N,t}e^{h_{N,t}}\big)\big)\,,$$

with (ρ_i, σ_i^2) set as in case (1) and $\nu = (2.5,\, 3,\, 4)$ as in case (2). Simulated samples are retained only if the post-burn-in kurtosis of each structural component is at least 3.6.

4. **Homoskedastic.**

$$\omega_{i,t} \equiv 1, \qquad h_{i,t} \equiv 0, \qquad \varepsilon_t \sim \mathcal{N}(0,\ I_N)\,,$$

so that the innovation variances remain constant over time.

To evaluate density forecast performance in the Monte Carlo simulation, we follow Clark (2011) and Carriero et al. (2024) and compute one-step-ahead predictive log scores. For each replication $r = 1, \ldots, R$, and for each forecast origin t, the predictive log score of model M is

$$\ell_{t+1}^{(r)}(M) = \log p_M(y_{t+1}^{(r)} \mid \mathcal{F}_t^{(r)}), \tag{B.49}$$

where $p_M(y_{t+1}^{(r)} \mid \mathcal{F}_t^{(r)})$ denotes the model's predictive density evaluated at the realized value $y_{t+1}^{(r)}$. Following Geweke and Amisano (2010), the predictive density is obtained using the mixture-of-parameters representation,

$$\hat{p}_M(y_{t+1}^{(r)} \mid \mathcal{F}_t^{(r)}) = \frac{1}{S}\sum_{s=1}^{S} p\left(y_{t+1}^{(r)} \mid \theta^{(s)}, \mathcal{F}_t^{(r)}, M\right), \tag{B.50}$$

where $\{\theta^{(s)}\}_{s=1}^{S}$ are posterior draws of the model parameters and latent states. This mixture-of-parameters approach integrates the conditional predictive densities over the posterior distribution of the parameters, providing an exact evaluation of the predictive density implied by the MCMC output and avoiding additional simulation noise when computing log scores.

For each replication, the individual predictive log scores are summed over all forecast origins to form the total log predictive likelihood of model M_j:

$$\mathrm{LPL}^{(r)}(M_j) = \sum_{t=T_0}^{T-1} \ell_{t+1}^{(r)}(M_j). \tag{B.51}$$

The difference between the total log predictive likelihoods of two models provides the predictive log Bayes factor:

$$\log \mathrm{BF}_{i0}^{(r)} = \mathrm{LPL}^{(r)}(M_i) - \mathrm{LPL}^{(r)}(M_0), \tag{B.52}$$

where M_0 denotes the benchmark model. A positive value of $\log \mathrm{BF}_{i0}^{(r)}$ indicates that model M_i assigns higher probability density to the realized data and thus delivers superior density forecasts in replication r.

To summarize results across replications, the total log predictive likelihoods and predictive log Bayes factors are averaged over the replications included in the pooled summary:

$$\overline{\mathrm{LPL}}(M_j) = \frac{1}{R} \sum_{r=1}^{R} \mathrm{LPL}^{(r)}(M_j), \tag{B.53}$$

$$\overline{\log \mathrm{BF}}_{i0} = \frac{1}{R} \sum_{r=1}^{R} \log \mathrm{BF}_{i0}^{(r)}. \tag{B.54}$$

Here R denotes the number of replications used for the corresponding DGP-model combination, set to 200 for all simulation designs. These averages provide a measure of the expected cumulative forecast performance of each model across simulated samples. Following Lütkepohl and Schlaak (2018) and Bertsche and Braun (2022), results are reported as Monte Carlo averages across 200 replications, with statistics computed for each simulated dataset and then averaged across replications. Each simulated dataset contains $T = 500$ monthly observations (about forty years), and one-step-ahead forecasts are generated recursively after an initial estimation window of 240 observations (about twenty years) until the end of the sample. Higher values of $\overline{\mathrm{LPL}}(M)$ or $\overline{\log \mathrm{BF}}_{i0}$ indicate superior overall density forecast accuracy.

The Monte Carlo simulation delivers two main findings. First, in terms of density fit, the SV-t specification performs consistently well across all four DGPs and attains the highest mean predictive log likelihood in each case. Its advantage over the correctly matched simpler specification is nevertheless modest under the SV and t-Distribution

DGPs. This pattern reflects the complementarity of its two components: persistent stochastic volatility captures low-frequency shifts in the variance environment, while heavy-tailed innovations accommodate occasional extreme realisations that would otherwise distort the predictive density. The additional flexibility of the SV-t specification therefore appears to impose only a limited cost when the true DGP contains just one of these features. Because the reported results are based on a finite number of Monte Carlo replications, the small quantitative differences across specifications may vary somewhat in a larger simulation. The broad ranking of the models, however, is stable across the replications considered. In empirical applications where the variance process is unknown, the SV-t specification consequently provides a useful general specification.

Second, and more importantly, structural identification is substantially more robust than density fit. Figure B.1 reports the true and estimated impulse responses for representative Monte Carlo replications under the SV, SV-t, and t-Distribution DGPs. The SV, SV-t, and t-Distribution specifications all recover the true impulse responses closely across most response-shock combinations, even when the estimated variance model differs from the true DGP. An SV model estimated on data generated by a t-Distribution DGP, and a t-Distribution model estimated on SV data, both track the true IRFs accurately. This cross-DGP robustness reflects the underlying identification logic: what matters is not the exact parametrization of the variance process, but whether the data contain sufficient identifying variation through heteroskedasticity, non-Gaussianity, or both. Once the DGP features time variation in variances or excess kurtosis, the rotational indeterminacy of the Gaussian homoskedastic model is broken, and any specification that captures the relevant variation in second moments or excess kurtosis delivers similar structural conclusions. By contrast, the homoskedastic specification displays visibly larger deviations from the true IRFs and wider uncertainty bands, particularly for responses where the true dynamics are sizeable. In a homoskedastic Gaussian environment the likelihood is invariant to orthogonal rotations, so the impact matrix is not uniquely pinned down and the identification fails. The comparison of the heteroskedastic and homoskedastic results therefore isolates the source of identification: it is the distributional variation in the data, not the specific variance model, that identifies the structural shocks.

Taken together, the two findings carry a clear methodological implication: reliable structural identification does not require correctly specifying the exact volatility dynamics. What matters is that the data contain sufficient identifying variation through changes in second moments, excess kurtosis, or both. Once this variation is present, alternative variance specifications deliver consistent structural conclusions, even though they may differ meaningfully in their density fit. These findings carry over directly to the empirical application. Although the estimated variance processes differ meaningfully across the SV, SV-t, and Homoskedastic-t specifications, all three recover nearly identical structural impulse responses. This suggests that the financial data contain sufficiently rich identifying variation for structural inference to be robust across alternative heteroskedastic specifications.

Table B.1: Mean predictive log likelihoods.

DGP	SV	SV-t	t-Distribution
SV	-1258.58	-1245.47	-1288.14
SV-t	-1487.66	-1475.89	-1507.17
t-Distribution	-1269.32	-1261.61	-1271.50
Homoskedastic	-1052.31	-1045.34	-1060.82

Notes: Entries are mean one-step-ahead predictive log likelihoods. Rows correspond to data-generating processes (DGPs), columns to estimated models. Higher (less negative) values indicate better density forecast performance.

Figure B.1: True versus estimated impulse responses in representative Monte Carlo replications.

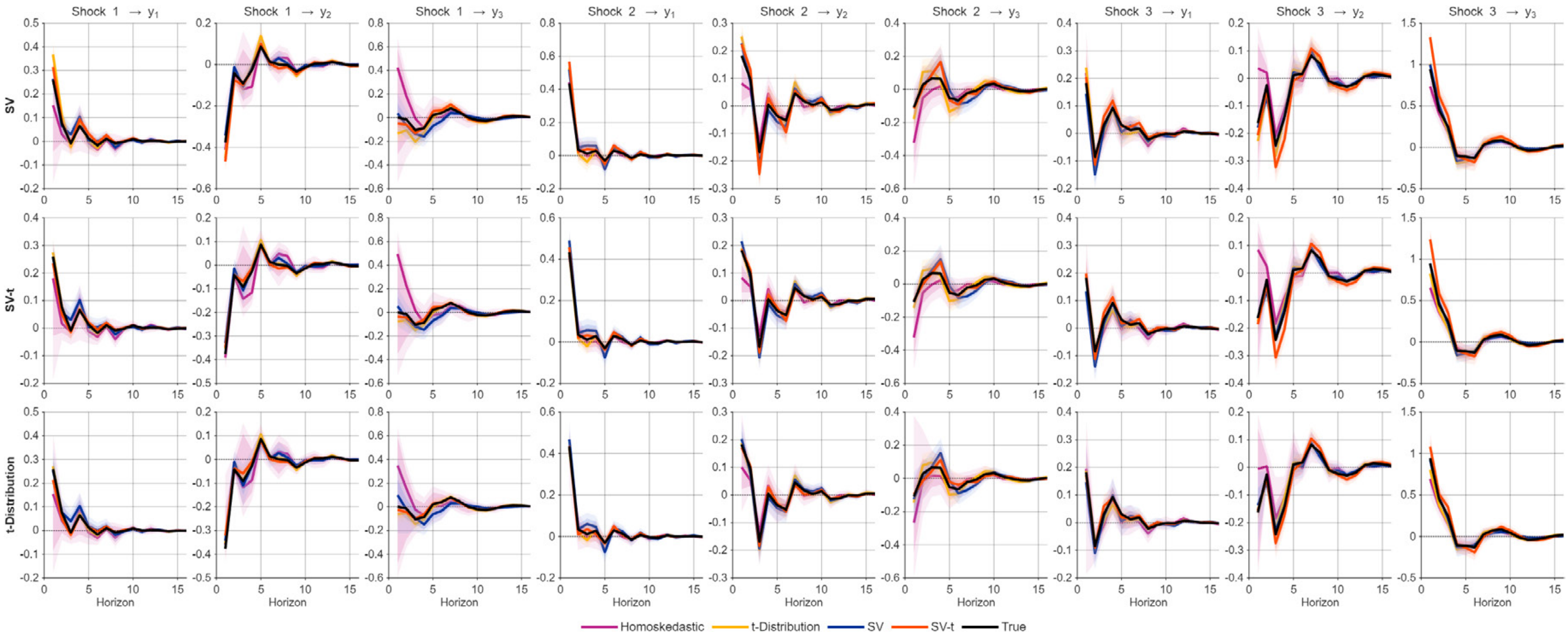

Notes: The figure reports impulse responses for the three-variable VAR used in the Monte Carlo simulation. Rows correspond to representative replications from the SV, SV-t, and t-Distribution DGPs, while columns correspond to the nine response-shock combinations. Within each panel, the coloured lines denote posterior median impulse responses from the alternative estimated models, and the shaded areas report the corresponding posterior credible intervals. The dashed black line denotes the true impulse response implied by the common VAR dynamics and impact matrix. Parameter draws are normalised using the true impact matrix.

B.1 Predictive log likelihood calculations

The predictive log likelihood implied by the one-step-ahead predictive density can be constructed recursively. As in Geweke and Amisano (2010), we start from the following decomposition, where M_j denotes model j and y^t are the data up to and including time t:

$$\log(p(y^T|M_j)) = \sum_{t=1}^{T} \log(p(y_t|y^{t-1}, M_j)) \tag{B.55}$$

Hence, to evaluate the predictive log likelihood one simply sums the individual one-step-ahead out-of-sample predictive density evaluations. However, the fact that the decomposition is based on out-of-sample predictive densities makes it impractical for all time periods of the sample. It is common practice to start the summation at some sufficiently large time point and instead calculate:

$$\log(p(y^T|y^{T_0}, M_j)) = \sum_{t=T_0+1}^{T} \log(p(y_t|y^{t-1}, M_j)) \tag{B.56}$$

If T_0 is sufficiently large the influence of the prior on the predictive densities is small and the data dominate in the model comparison. The remaining step is to evaluate the predictive density conditional on each recursive sample y^{t-1}, which can be written as

$$p\left(y_t|y^{t-1}, M_j\right) = \int_{\Theta_j} p\left(y_t|y^{t-1}, \Theta_j, M_j\right) p\left(\Theta_j|y^{t-1}, M_j\right) \mathrm{d}\Theta_j \tag{B.57}$$

$$\approx \frac{1}{S}\sum_{s=1}^{S} p\left(y_t|y^{t-1}, \Theta_j^{(s)}, M_j\right) \tag{B.58}$$

where S is a MCMC sample with which one can approximate the exact integral over the parameters Θ_j of model j.

It remains to show how we evaluate the predictive densities, for which we first define $\log\left(p\left(y_t|y^{t-1}, M_j\right)\right) \equiv L(s,j)$ for the different models. First, we recap the model for convenience:

$$y_t = B'x_t + A^{-1}O_t^{1/2}v_t \tag{B.59}$$

$$\Rightarrow v_t = O_t^{-1/2}A(y_t - B'x_t) \tag{B.60}$$

$$O_t = diag(e^{h_{1,t}}, \ldots, e^{h_{N,t}}) \tag{B.61}$$

where x_t contains the relevant data until time $t-1$ and $B'x_t$ denotes the conditional mean of y_t given the data and parameters. With parameter draws for A, B, h, and ν, as well as the out-of-sample observations y_t, one can compute all terms above. Values for $h_{i,t}$ can be generated from the individual autoregressive processes above.

When the model includes stochastic volatility but not heavy tails, v_t follows a multivariate standard normal distribution. The predictive density is therefore

$$L(s,j) = -\frac{N}{2}\log(2\pi) - \frac{1}{2}\log(\det(V_y)) - \frac{1}{2}(y_t - B'x_t)'V_y^{-1}(y_t - B'x_t) \tag{B.62}$$

$$V_y = A^{-1}O_t\left(A^{-1}\right)' \tag{B.63}$$

The determinant term in V_y incorporates the Jacobian of the transformation from the structural shocks to y_t.

When the model includes heavy-tailed shocks, the elements of v_t follow independent Student-t distributions with ν_i degrees of freedom. The absolute value of the determinant of the Jacobian of the inverse transformation from ϵ_t to y_t is simply $O_t^{-1/2}|\det(A)|$. Hence, the predictive density conditional on parameters in this case is:

$$\begin{aligned} L(s,j) = \log(|\det(A)|) - \frac{1}{2}\sum_{i=1}^{N} h_{i,t} \\ + \sum_{i=1}^{N}\left[\log(\Gamma((\nu_i+1)/2)) - \log(\Gamma(\nu_i/2)) - \frac{1}{2}\log(\pi\nu_i)\right] \\ - \sum_{i=1}^{N}\frac{\nu_i+1}{2}\log\left(1+\frac{\epsilon_{i,t}^2}{\nu_i}\right) \end{aligned} \tag{B.64}$$

The structural errors are calculated from the model equations above. When stochastic volatility is not present in the model we have $h_{1,t} = \cdots = h_{N,t} = 0$.

Once we have calculated $L(s,j)$ for every s we need to take the average over the exponentials of these values. To do so in a numerically stable way we again use the

"LogSumExp" trick:

$$\log\left(p\left(y_t|y^{t-1},M_j\right)\right) \approx \log\left(\frac{1}{S}\sum_{s=1}^{S} p\left(y_t|y^{t-1},\Theta_j^{(s)},M_j\right)\right) \tag{B.65}$$

$$= \log\left(\frac{1}{S}\sum_{s=1}^{S} \exp\left(L(s,j)\right)\right) \tag{B.66}$$

$$= \log\left(\frac{1}{S}\sum_{s=1}^{S} \exp\left(L(s,j)-L^*\right)\right) + L^* \tag{B.67}$$

$$L^* = \max_s\{L(s,j)\} \tag{B.68}$$

When stochastic volatility is present, to improve the accuracy of the computations, for each s we simulate 100 values for $h_{i,t}$ and expand the average across these additional draws.

C Application to Oil Price Data

This section follows the empirical set-up of Bertsche and Braun (2022) and applies our model to the same four-variable oil market VAR. The dataset consists of monthly observations for 1974:01–2016:12 and is specified as

$$y_t = \Big[100\Delta q_t,\ 100\Delta wip_t,\ 100p_t,\ 100\Delta inv_t\Big]',$$

where q_t denotes global crude oil production (in million barrels per day), wip_t is world industrial production following Baumeister and Hamilton (2019), p_t is the real WTI oil price, and Δinv_t captures changes in global oil inventories. All series enter the VAR in log-levels or log-differences as appropriate. We use twelve lags, consistent with the literature, and exclude pre-1974 observations when U.S. oil prices were regulated.

The analysis compares the results of Bertsche and Braun (2022) with three variants of the model proposed in this paper:

1. a t-Distribution specification,
2. an SV specification, and
3. an SV-t specification.

Figure C.2 presents impulse responses for the conventional oil supply shock under all three variants. The t-Distribution model aligns closely with the frequentist stochastic-volatility benchmark of Bertsche and Braun (2022), confirming that modelling fat-tailed structural shocks provides a parsimonious way of accommodating extreme observations and delivers impulse responses that are empirically similar to those obtained under heteroskedastic identification.
Across all variables, the SV, t-Distribution, and SV-t models produce very similar impulse responses. Consistent with Bertsche and Braun (2022), structural inference is robust when the data contain sufficiently informative variation in second moments, excess kurtosis, or both. The t-Distribution model is particularly noteworthy: despite its parsimony—adding only a single degrees-of-freedom parameter per equation—it reproduces essentially the same dynamic responses as the richer SV specification. The conventional oil supply shock (shock 1) produces a decline in production, a fall in world industrial activity, and an increase in real oil prices, in line with Känzig (2021) and the benchmark responses in Bertsche and Braun (2022). The oil price news shock (shock 3)

raises real oil prices without an immediate decline in production and induces inventory adjustment over the medium term, again closely matching the patterns in Bertsche and Braun (2022). The fact that these qualitative and quantitative features are reproduced under all three specifications indicates that the empirical conclusions are robust across alternative specifications of the structural-shock distribution, even when using the more parsimonious t-Distribution model.

Figure C.3 compares the estimated log-volatilities under our Bayesian specifications with those obtained by Bertsche and Braun (2022). The volatility paths are remarkably similar across approaches, with pronounced spikes coinciding with well-known geopolitical and energy-market events. This reinforces the conclusion that the substantive economic interpretation is robust to alternative specifications of the structural-shock distribution. Volatility in oil production rises sharply during the oil crises of the 1970s and again around the Gulf War and the 2008 financial crisis. World industrial production volatility mirrors global business-cycle fluctuations, with frequent swings in the 1970s–1980s, relative stability during the 1990s aside from the Asian crisis, and a marked surge in 2008–09. Oil price volatility is highly sensitive to energy-market disruptions and geopolitical tensions, exhibiting extreme values in the 1970s, elevated levels in the 1980s, and strong increases in the 2000s. Inventory volatility remains comparatively subdued, consistent with its role in buffering short-run demand–supply imbalances.

Figure C.4 shows that the posterior degrees of freedom vary markedly across equations. In the t-Distribution specification, low degrees of freedom are most evident for oil production, world industrial production, and inventories, while the real oil price equation is associated with substantially higher values. Once stochastic volatility is introduced in the SV-t specification, the evidence for heavy tails becomes more selective, remaining most pronounced for world industrial production and weakening for the other equations. This pattern suggests that part of the apparent non-Gaussianity in the shocks reflects time-varying volatility, so that the role of the Student-t component is heterogeneous across variables and partly subsumed by stochastic volatility.

Figure C.2: Impulse responses for oil supply shocks.

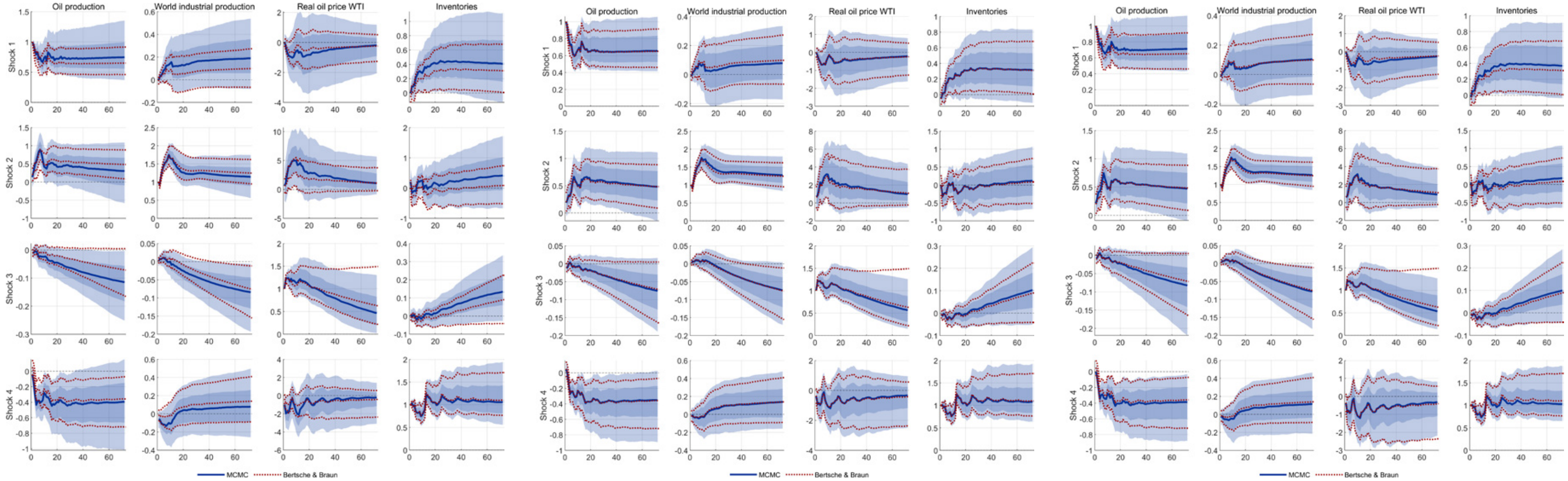

(a) T-Distribution **(b)** SV **(c)** SV-t

Notes: Impulse responses to oil supply shocks up to a horizon of 72 months. Panels (a)–(c) report results from the T-distribution, stochastic volatility (SV), and combined SV-t specifications, respectively. Solid blue lines denote posterior median impulse responses, while the shaded areas represent 68% and 95% posterior credible intervals. Red dotted lines report the corresponding responses from Bertsche and Braun (2022).

Figure C.3: Estimates of log volatilities.

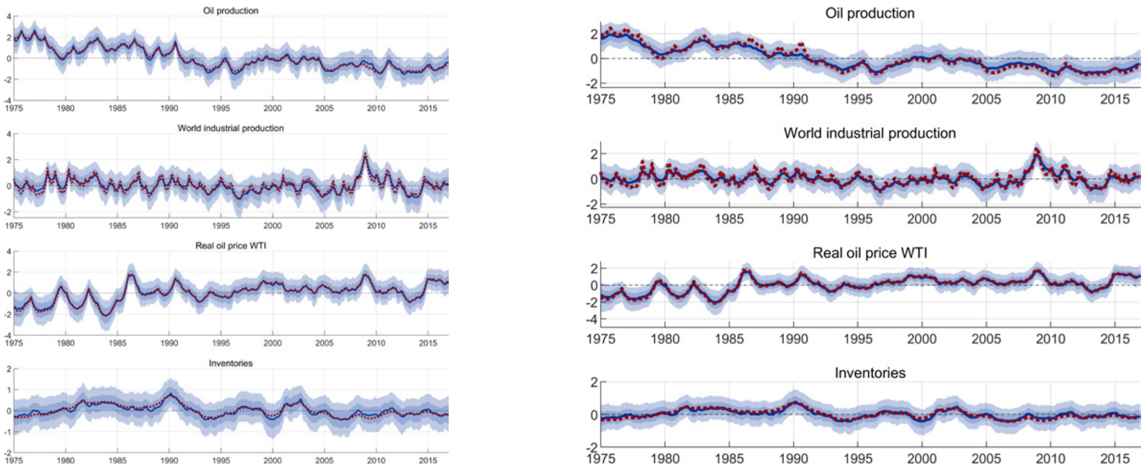

(a) SV **(b)** SV-t

Notes: The figure reports Bayesian estimates of the log-volatility process $h_{i,t}$ for each variable. The dark blue line denotes the posterior median, while the darker and lighter shaded areas represent the 68% and 95% posterior credible intervals, respectively. The red dotted line reports the corresponding frequentist estimate from Bertsche and Braun (2022).

Figure C.4: Posterior degrees of freedom.

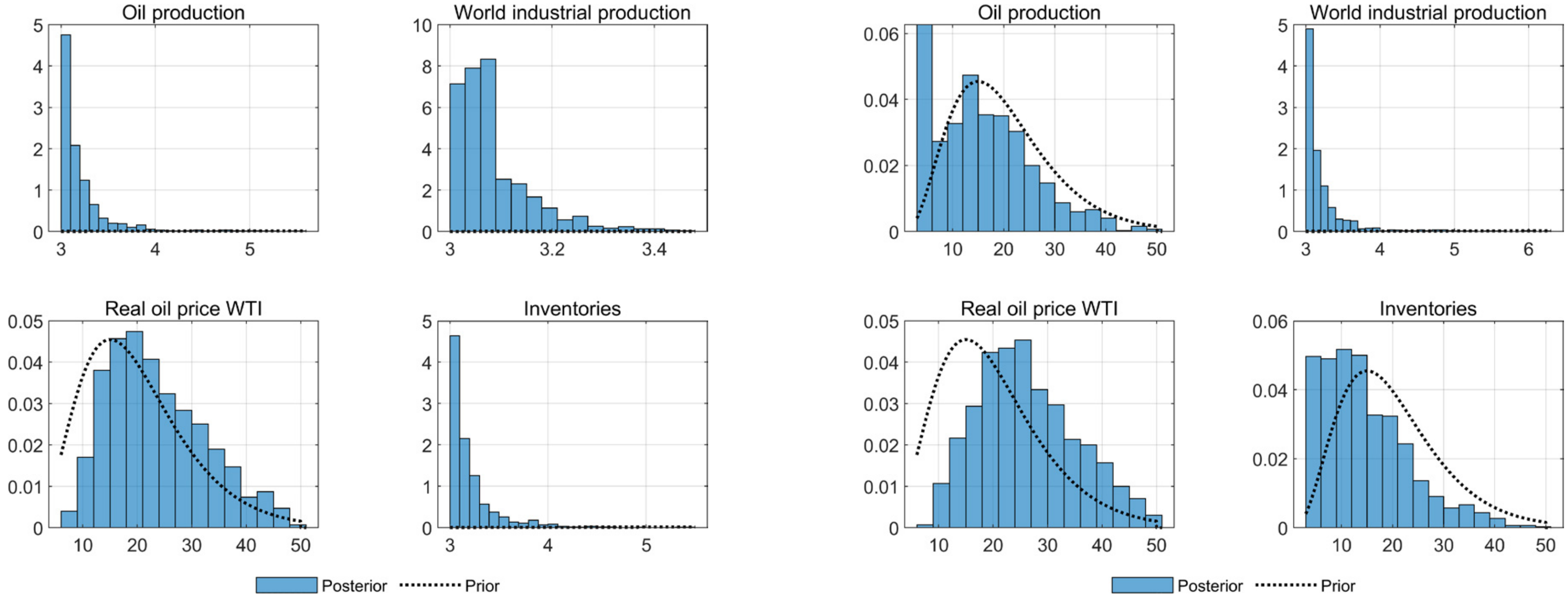

(a) T-Distribution **(b)** SV-t

Notes: Histograms of posterior draws of the degrees of freedom of each structural shock. The dashed line corresponds to the prior distribution evaluated at grid points covering the posterior draws.

D Additional Results: Financial Market Dynamics Around the 2025 Tariff Announcement

This section reports additional results supporting the empirical analysis of financial-market dynamics around the April 2025 tariff announcement. Table D.2 summarizes the ten endogenous variables in the baseline model.

Table D.2: Data description, transformations, and sources

	Series	Definition	Transf.	Key	Source
1	S&P 500	Broad U.S. equity price index	log ×100	SPX	Refinitiv
2	VIX	Chicago Board Options Exchange implied volatility index (percent)	level	VIXCLS	FRED
3	EUR per USD exchange rate	Euros per U.S. dollar; constructed as the inverse of the euro–dollar rate (dollars per euro)	log ×100	EUR=	Refinitiv
4	π_{1Y}^{swap}	One-year U.S. inflation-linked swap rate (percent)	level	USCPIZ1Y=	Refinitiv
5	Treasury term premium (3M)	Three-month U.S. Treasury term premium from the Adrian–Crump–Moench (ACM) model (percent)	level	—	Adrian et al. (2013)
6	US 10Y yield	Ten-year U.S. Treasury benchmark yield (percent)	level	US10YT=RR	Refinitiv
7	EA 10Y yield	Ten-year euro-area benchmark government bond yield, proxied by the German Bund (percent)	level	DE10YT=RR	Refinitiv
8	Swap spread (10Y)	Ten-year USD interest rate swap rate minus ten-year U.S. Treasury yield (percentage points)	level	—	Constructed
9	Dollar convenience (10Y)	Ten-year G10 benchmark CIP deviation; daily cross-currency median, 13-day moving average (basis points)	level	—	Du et al. (2026, 2018a)
10	Treasury convenience (10Y)	G10 median ten-year government-bond CIP deviation; 13-day moving average (basis points)	level	—	Du et al. (2018a, 2026)

Notes: The estimation sample runs from 2 July 2007 to 15 May 2025 at daily frequency. The table reports the ten endogenous variables of the VAR specification (Model C-VIII). The EUR per USD exchange rate is constructed as the inverse of the euro–dollar rate so that the series rises with dollar appreciation. The three-month Treasury term premium follows the ACM estimation procedure in Adrian et al. (2013). The Swap spread (10Y) is computed as the difference between the ten-year USD swap rate and the ten-year U.S. Treasury yield. Dollar convenience (10Y) is available from January 2008. *Transf.* denotes the transformation applied prior to estimation: equity and exchange-rate series enter in log levels multiplied by 100, while yields, spreads, term-premium estimates, and CIP deviations enter in levels (percent or basis points as indicated). FRED refers to the Federal Reserve Economic Data database.

Swap–Treasury Spread (10Y). The ten-year Swap–Treasury spread is defined as the fixed rate on a ten-year U.S. dollar interest rate swap minus the ten-year U.S. Treasury benchmark yield:

$$\text{Swap–Treasury spread}_{n,t} = y^{\text{swap}}_{n,t} - y^{\text{UST}}_{n,t}.$$

The spread compares two ways of obtaining duration exposure—through swaps or by holding cash Treasuries. A higher spread indicates that Treasuries are expensive relative to swaps; a more negative spread indicates that Treasuries are cheap relative to swaps, which is commonly associated with limits to arbitrage, dealer balance-sheet constraints, and impaired Treasury-market intermediation (Boyarchenko et al., 2018; Kashyap et al., 2025). After the Global Financial Crisis, swap spreads in the U.S. turned persistently negative, a pattern that deepened further around the March 2020 Treasury-market turmoil and again in 2025 (Du et al., 2026).

Dollar Convenience (10Y). Dollar Convenience is the benchmark covered interest parity (CIP) deviation as defined in Du et al. (2018b) and Du et al. (2026). It compares the return on a synthetic dollar risk-free asset—obtained by investing in a foreign risk-free instrument and hedging the exchange-rate risk through an FX swap—with the return on a cash-market dollar risk-free asset at the same maturity:

$$x^{Rf}_{i,n,t} = \underbrace{\left(y^{Rf}_{i,n,t} - \rho_{i,n,t}\right)}_{\text{FX-swap-implied dollar rate}} - \underbrace{y^{Rf}_{\$,n,t}}_{\text{cash-market dollar rate}}$$

where $\rho_{i,n,t}$ is the forward premium required to hedge currency i into dollars. A positive value ($x^{Rf} > 0$) indicates that cash dollar assets are more convenient than foreign synthetic dollar assets, reflecting the non-pecuniary services—liquidity, collateral value, reserve-currency status—that investors derive from holding dollar-denominated safe assets. A negative value indicates the reverse. The series is constructed as the G10 cross-currency median, smoothed with a 13-day moving average, at the ten-year horizon. An important construction detail concerns the post-LIBOR transition: prior to July 2023, the dollar risk-free rate was proxied by LIBOR; following the discontinuation of LIBOR, the series uses SOFR-based rates, following the methodology in Du et al. (2026) to ensure continuity of the benchmark. The series is available from January 2008 and is sourced from the data page of Wenxin Du.[2]

Treasury Convenience (10Y). Treasury Convenience is the government-bond CIP deviation as defined in Du et al. (2018a) and Du et al. (2026). It compares the swapped return on foreign government bonds with the yield on U.S. Treasuries at the same maturity:

$$x_{i,n,t}^{Govt} = \underbrace{\left(y_{i,n,t}^{Govt} - \rho_{i,n,t}\right)}_{\text{foreign government yield swapped into dollars}} - \underbrace{y_{\$,n,t}^{Govt}}_{\text{U.S. Treasury yield}}$$

A positive value indicates that U.S. Treasuries are more convenient than foreign government bonds; a negative value indicates the reverse. This measure isolates the Treasury-specific component of U.S. safe-asset demand from broader dollar convenience. Like Dollar Convenience, it is computed as the G10 median smoothed with a 13-day moving average, and is sourced from the data page of Wenxin Du. Du et al. (2026) show that dollar convenience and Treasury convenience have become increasingly distinct—particularly following the post-crisis restructuring of Treasury markets—making it important to include both measures to separately track changes in global demand for dollar assets from disruptions specific to Treasury-market intermediation.

Figures D.5 and D.6 provide diagnostic evidence relevant to the statistical identification. Figure D.5 reports the estimated stochastic volatility processes together with the posterior distributions of the Student-t degrees-of-freedom parameters, while Figure D.6 reports MCMC trace plots for the normalised impact-matrix coefficients. Together, these diagnostics indicate that the data contain substantial variation in second moments and excess kurtosis, supporting the statistical identification strategy.

The combined safe-haven component is the sum of shocks 1 and 2; around early April 2025, this sum accounts for the initial conventional risk-off response.

[2] `sites.google.com/site/wenxindu/data`.

Figure D.5: Heteroskedasticity and Non-Gaussianity Metrics

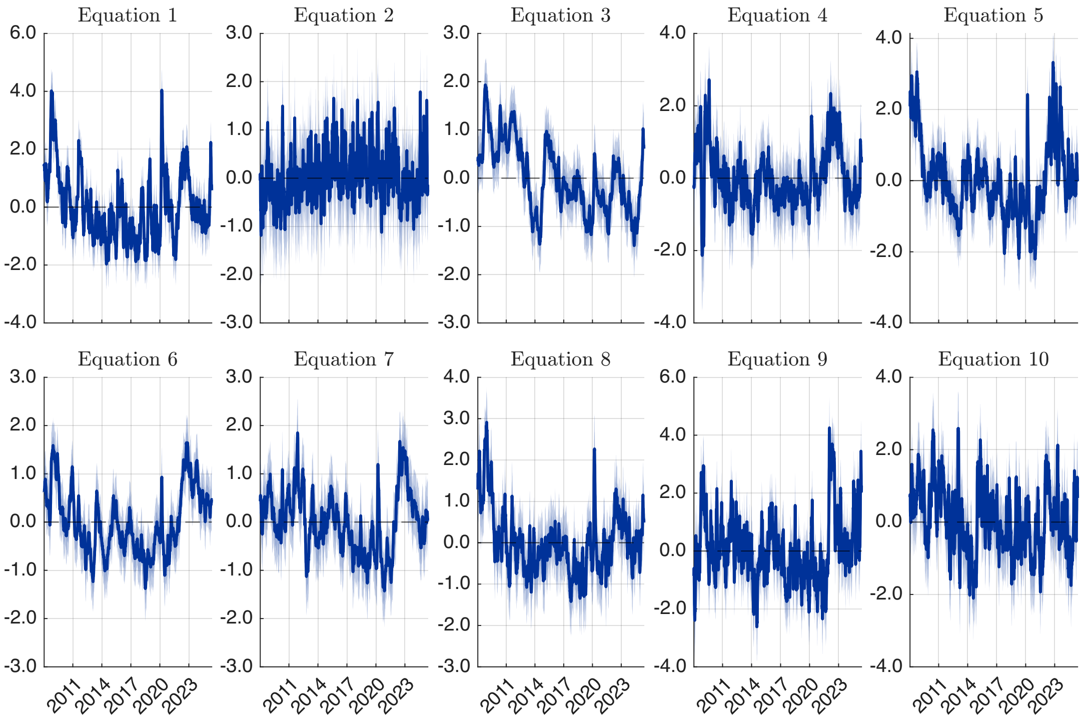

(a) Stochastic volatility

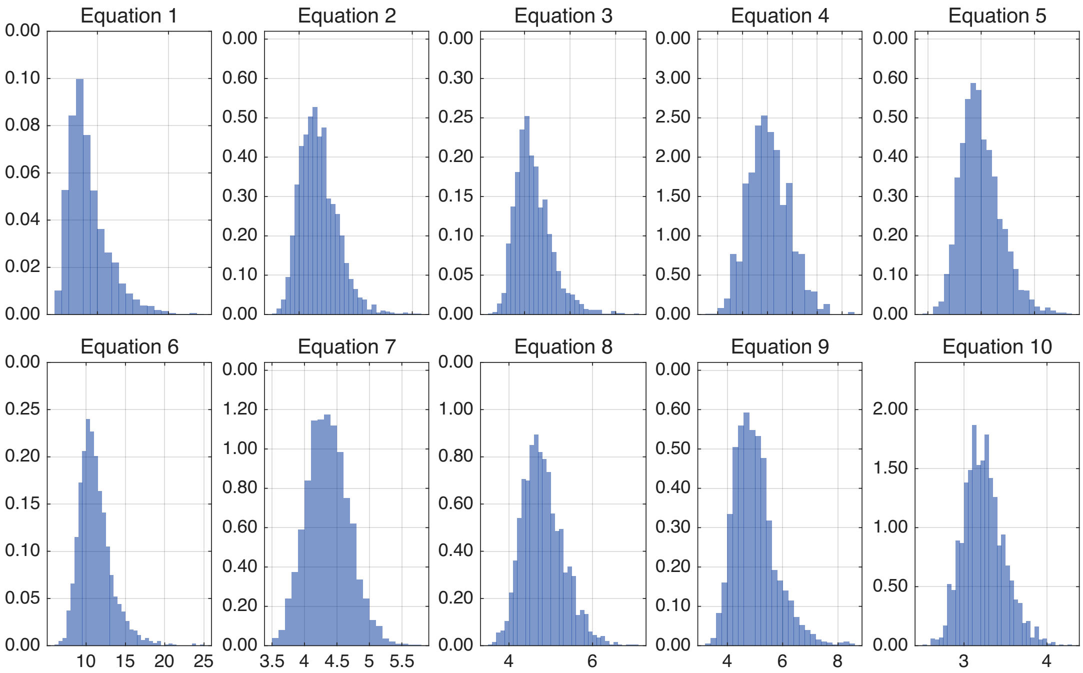

(b) Student-t degrees of freedom

Notes: The figure reports heteroskedasticity metrics from the SV-t model. Panel (a) displays estimated log-volatility for each structural shock. Shaded areas represent 68% and 95% posterior intervals. Panel (b) reports posterior distributions for the degrees-of-freedom parameter ν associated with each shock.

Figure D.6: Posterior draws of the normalised impact matrix

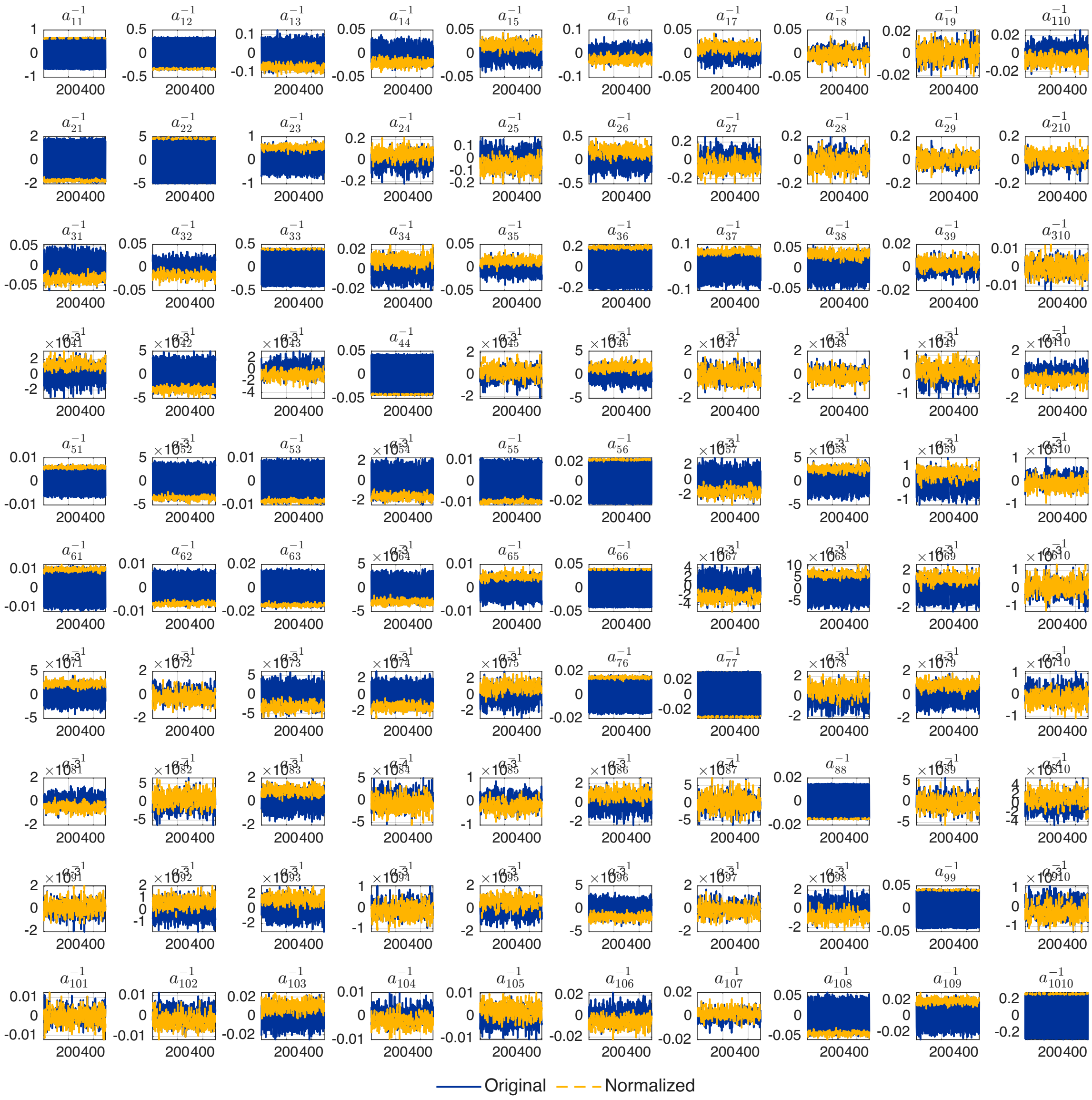

Figure D.7: Impulse response functions to all identified structural shocks

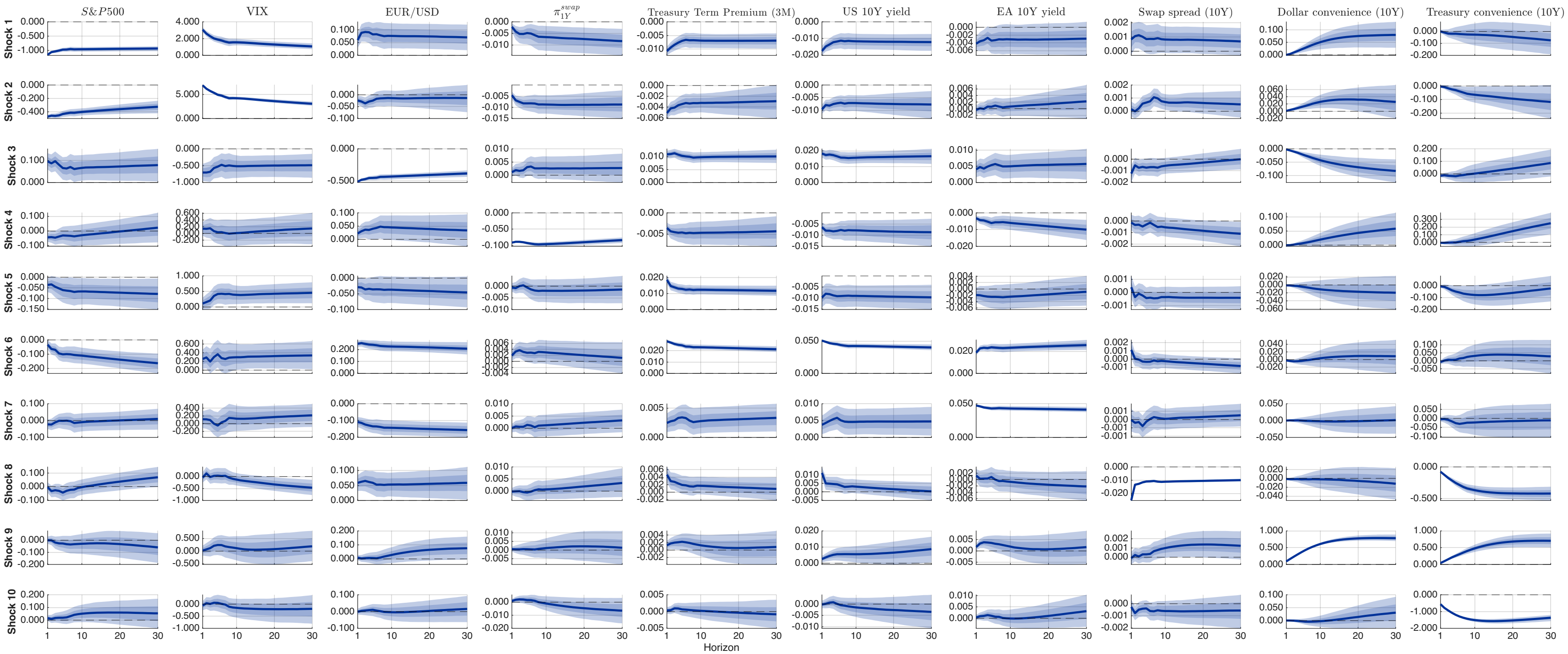

Notes: The figure presents impulse response functions to all ten statistically identified structural shocks over a horizon of 30 days. Shaded areas denote 68% and 95% pointwise posterior intervals.

Figure D.8: Shock-by-shock historical decomposition

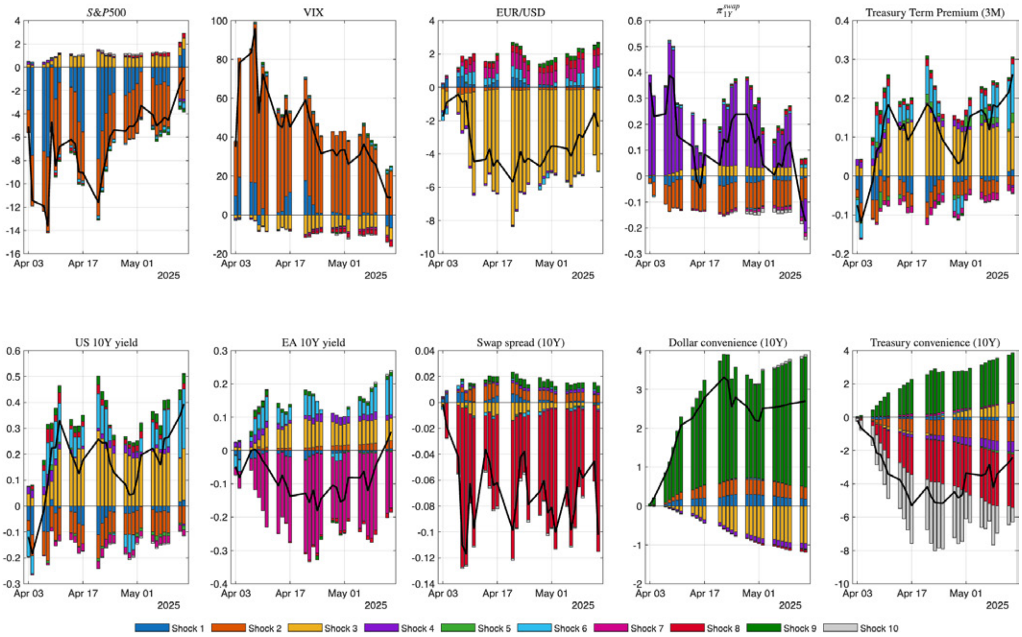

(a) April 2025 tariff announcement

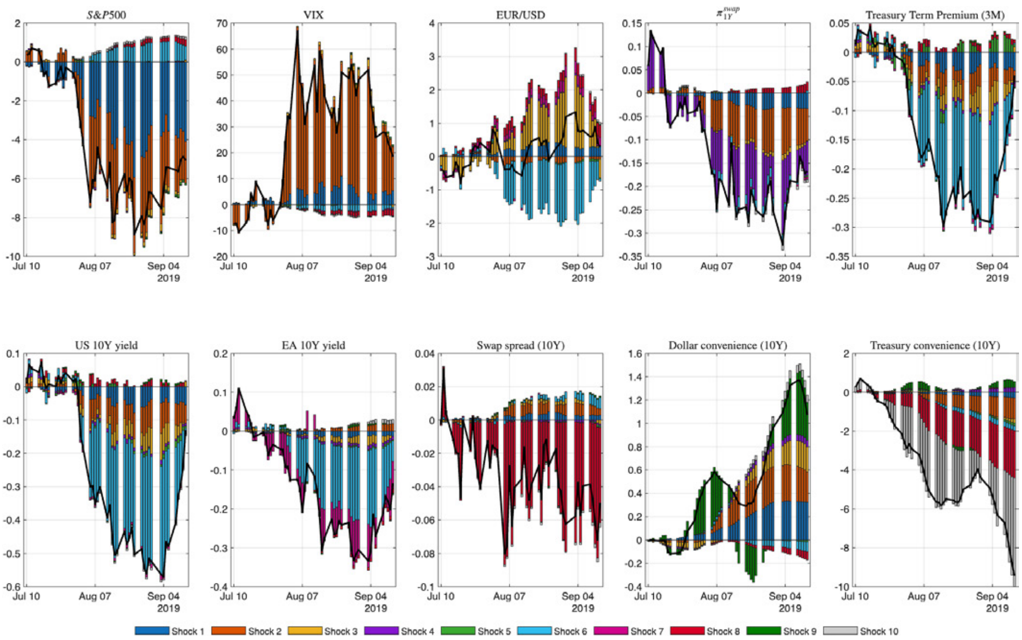

(b) August 2019 tariff escalation

Notes: Panel (a) reports the shock-by-shock historical decomposition for observations from 2 April to 14 May 2025, conditional on the initial observation on 2 April. Panel (b) reports the corresponding decomposition for observations from 9 July to 15 September 2019, conditional on the initial observation on 9 July. Stacked bars show the cumulative contributions of the statistically identified structural shocks; the black line denotes the explained component, measured as the deviation from the deterministic component. *Safe-Haven shock* = shocks 1–2; *U.S. Institutional Credibility shock* = shock 3; *Treasury Market Intermediation shock* = shock 8; *Safe-Asset Convenience shock* = shock 9; Other shocks = shocks 4–7 and 10.

BANCO DE ESPAÑA PUBLICATIONS

WORKING PAPERS

2520 ALICIA AGUILAR: Beyond fragmentation: unraveling the drivers of yield divergence in the euro area.

2521 RUBÉN DOMÍNGUEZ-DÍAZ and DONGHAI ZHANG: The macroeconomic effects of unemployment insurance extensions: A policy rule-based identification approach.

2522 IRMA ALONSO-ALVAREZ, MARINA DIAKONOVA and JAVIER J. PÉREZ: Rethinking GPR: The sources of geopolitical risk.

2523 ALBERTO MARTÍN, SERGIO MAYORDOMO and VICTORIA VANASCO: Banks vs. Firms: Who Benefits from Credit Guarantees?

2524 SUMIT AGARWAL, SERGIO MAYORDOMO, MARÍA RODRÍGUEZ-MORENO and EMANUELE TARANTINO: Household Heterogeneity and the Lending Channel of Monetary Policy.

2525 DIEGO BONELLI, BERARDINO PALAZZO, and RAM YAMARTHY: Good inflation, bad inflation: implications for risky asset prices.

2526 STÉPHANE BONHOMME and ANGELA DENIS: Fixed Effects and Beyond. Bias Reduction, Groups, Shrinkage and Factors in Panel Data.

2527 ÁLVARO FERNÁNDEZ-GALLARDO and IVÁN PAYÁ: Public debt burden and crisis severity.

2528 GALO NUÑO: Three Theories of Natural Rate Dynamics.

2529 GALO NUÑO, PHILIPP RENNER and SIMON SCHEIDEGGER: Monetary policy with persistent supply shocks.

2530 MIGUEL ACOSTA-HENAO, MARÍA ALEJANDRA AMADO, MONTSERRAT MARTÍ and DAVID PÉREZ-REYNA: Heterogeneous UIPDs across Firms: Spillovers from U.S. Monetary Policy Shocks.

2531 LUIS HERRERA and JESÚS VÁZQUEZ: Learning from news.

2532 MORTEZA GHOMI, JOCHEN MANKART, RIGAS OIKONOMOU and ROMANOS PRIFTIS: Debt maturity and government spending multipliers.

2533 MARINA DIAKONOVA, CORINNA GHIRELLI and JAVIER J. PÉREZ: Political polarization in Europe.

2534 NICOLÁS FORTEZA and SERGIO PUENTE: Measuring non-workers' labor market attachment with machine learning.

2535 GERGELY GANICS and LLUC PUIG CODINA: Simple Tests for the Correct Specification of Conditional Predictive Densities.

2536 HENRIQUE S. BASSO and OMAR RACHEDI: Robot adoption and inflation dynamics.

2537 PABLO GARCIA, PASCAL JACQUINOT, ČRT LENARČIČ, KOSTAS MAVROMATIS, NIKI PAPADOPOULOU and EDGAR SILGADO-GÓMEZ: Green transition in the Euro area: domestic and global factors.

2538 MARÍA ALEJANDRA AMADO, CARLOS BURGA and JOSÉ E. GUTIÉRREZ: Cross-border spillovers of bank regulations: Evidence of a trade channel.

2539 ALEJANDRO CASADO and DAVID MARTÍNEZ-MIERA: Banks' specialization and private information.

2540 CHRISTIAN E. CASTRO, ÁNGEL ESTRADA GARCÍA and GONZALO FERNÁNDEZ DIONIS: Diversifying sovereign risk in the Euro area: empirical analysis of different policy proposals.

2541 RAFAEL GUNTIN and FEDERICO KOCHEN: The Origins of Top Firms.

2542 ÁLVARO FERNÁNDEZ-GALLARDO: Natural disasters, economic activity, and property insurance: evidence from weekly U.S. state-level data.

2543 JOSÉ ELÍAS GALLEGOS, ESTEBAN GARCÍA-MIRALLES, IVÁN KATARYNIUK and SUSANA PÁRRAGA RODRÍGUEZ: Fiscal Announcements and Households' Beliefs: Evidence from the Euro Area.

2544 LUIS HERRERA, MARA PIROVANO and VALERIO SCALONE: From risk to buffer: Calibrating the positive neutral CCyB rate.

2545 ESTEBAN GARCÍA-MIRALLES et al.: Fiscal drag in theory and in practice: A European perspective.

2546 TATSURO SENGA and IACOPO VAROTTO: Investment Irreversibility in a Granular World.

2547 OLYMPIA BOVER, NEZIH GUNER, YULIYA KULIKOVA, ALESSANDRO RUGGIERI and CARLOS SANZ: Family-friendly policies and fertility: What firms have to do with it?

2548 ADINA-ELENA FUDULACHE and MARIA DEL CARMEN CASTILLO LOZOYA: Demand drivers of central bank liquidity: A time-to-exit TLTRO analysis.

2549 ERIK ANDRES-ESCAYOLA, LUIS MOLINA, JAVIER J. PÉREZ and ELENA VIDAL: How economic policy uncertainty spreads across borders: the case of Latin America.

2550 MATTHIAS BURGERT, MATTHIEU DARRACQ PARIÈS, LUIGI DURAND, MARIO GONZÁLEZ, ROMANOS PRIFTIS, OKE RÖHE, MATTHIAS ROTTNER, EDGAR SILGADO-GÓMEZ, NIKOLAI STÄHLER and JANOS VARGA: Macroeconomic effects of carbon-intensive energy price changes: A model comparison.

2601 IACOPO VAROTTO: Blocking the Blockers? Diversity Matters.

2602 CARLOS CAÑIZARES MARTÍNEZ, ADRIANA LOJSCHOVÁ and ALICIA AGUILAR: Non-linear effects of monetary policy shocks on housing: Evidence from a CESEE country.

2603 DIEGO BONELLI: Inflation risk and yield spread changes.

2604 MARÍA ALEJANDRA AMADO: Macroprudential FX Regulations and Small Firms: Unintended Consequences for Credit Growth.

2605 FERNANDO ÁVALOS, BORIS HOFMANN and JOSE M. SERENA: Monetary policy and private equity acquisitions: tracing the links.

2606 RICARD GREBOL, MARGARITA MACHELETT, JAN STUHLER and ERNESTO VILLANUEVA: Assortative Mating, Inequality, and Rising Educational Mobility in Spain.

2607 PABLO AGUILAR, RUBÉN DOMÍNGUEZ-DÍAZ, JOSÉ-ELÍAS GALLEGOS and JAVIER QUINTANA: The Transmission of Foreign Shocks in a Networked Economy.

2608 ERWAN GAUTIER, CRISTINA CONFLITTI, DANIEL ENDERLE, LUDMILA FADEJEVA, ALEX GRIMAUD, EDUARDO GUTIÉRREZ, VALENTIN JOUVANCEAU, JAN-OLIVER MENZ, ALARI PAULUS, PAVLOS PETROULAS, PAU ROLDAN-BLANCO and ELISABETH WIELAND: Consumer price stickiness in the euro area during an inflation surge.

2609 MORTEZA GHOMI and SAMUEL HURTADO: RAUI: Uncertainty Indicators Built With Artificial Intelligence.

2610 MORTEZA GHOMI and EVI PAPPA: Stimulating avenues: EIB loans and returns to Public Investment.

2611 JUAN S. MORA-SANGUINETTI, CRISTINA PEÑASCO and ROK SPRUK: The impact of "Green Regulation" on firms' innovation.

2612 ÁLVARO FERNÁNDEZ-GALLARDO and EVI PAPPA: Natural disasters and fiscal shelters.

2613 NICOLÁS BONINO-GAYOSO and MÓNICA CORREA-LÓPEZ: Unexpecting the expected in real-time inflation forecasting: The inflation expectations channel?

2614 ANDRÉS AZQUETA-GAVALDÓN, MARINA DIAKONOVA, CORINNA GHIRELLI and JAVIER J. PÉREZ: Diverging signals from economic uncertainty measures: Uncovering coherence through news narratives.

2615 JOSÉ E. GUTIÉRREZ, ENRIC MARTORELL and MARIYA MELNYCHUK: The nexus between the deposit and risk-taking channels of monetary policy.

2616 MARTA GARCÍA-RODRÍGUEZ and CLEMENTE PINILLA-TORREMOCHA: The role of confidence measures in European unemployment dynamics.

2617 DANIEL DEJUAN-BITRIA: Processing forward-looking loan loss provisions: evidence from the adoption of the CECL model.

2618 RYAN BANERJEE, FRANCISCO GONZÁLEZ, JOSÉ E. GUTIÉRREZ and JOSE-MARÍA SERENA: Credit Supply in the Wake of Distressed Bank Acquisitions.

2619 ALEJANDRO CASADO, MARCO GIOMETTI, JOSÉ E. GUTIÉRREZ, DAVID MARTÍNEZ-MIERA, ALEXANDRA MATYUNINA and TAMMARO TERRACCIANO: Digitalization and credit markets: Evidence from e-Invoicing.

2620 JORGE ABAD, SAKI BIGIO, SALOMÓN GARCÍA-VILLEGAS, JOËL MARBET and GALO NUÑO: The Heterogeneous Bank Lending Channel of Monetary Policy.

2621 NICOLÁS FORTEZA and JOSÉ M. LABEAGA: Pollution, Density and Low Emission Zones: European Evidence.

2622 ANDREA DE POLIS, ÁLVARO FERNÁNDEZ-GALLARDO and JOSÉ NICOLÁS ROSAS: Oil supply shocks and inflation tail risks.

2623 LUIS HERRERA, CATERINA MENDICINO, KALIN NIKOLOV and VALERIO SCALONE: Monetary Tightening, Financial Stability and the Role of Macroprudential Policy.

2624 MARINA GÓMEZ-GARCÍA: The impact of air pollution on the housing market: The case of Madrid.

2625 ANA AGUILAR, RAFAEL GUERRA, CAROLA MÜLLER and ALEXANDRE TOMBINI: The macro-financial impact of economic policy uncertainty in Latin America.

2626 ANDREA DE POLIS, LEONARDO MELOSI and IVAN PETRELLA: The Taming of the Skew: Asymmetric Inflation Risk and Monetary Policy.

2627 EOGHAN O'NEILL and SOFIA VELASCO: Let the Tree Decide: FABART. A Non-parametric factor model for nonlinear oil shock transmission.

2628 CRAIG A. CHIKIS, JONATHAN GOLDBERG and DAVID LÓPEZ-SALIDO: The innovator's risk premium: Sticky hurdle rates, the cost of capital, and creative destruction.

2629 LUCAS TER STEEGE and SOFIA VELASCO: What volatility reveals: agnostic identification of exchange rate and Treasury-market dynamics in inconvenient times.